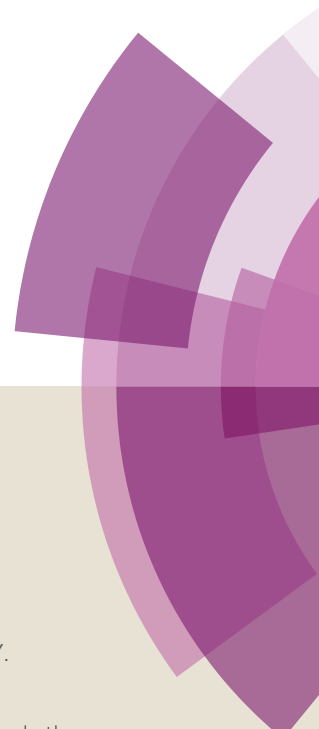
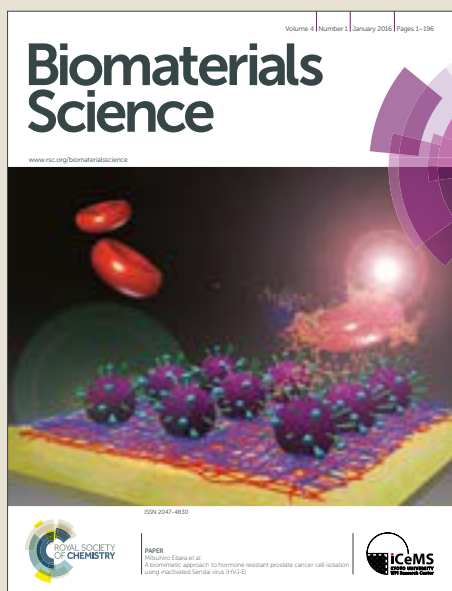


Biomaterials Science

Accepted Manuscript



This article can be cited before page numbers have been issued, to do this please use: M. Razavi and Y. Huang, *Biomater. Sci.*, 2019, DOI: 10.1039/C9BM00289H.



This is an Accepted Manuscript, which has been through the Royal Society of Chemistry peer review process and has been accepted for publication.

Accepted Manuscripts are published online shortly after acceptance, before technical editing, formatting and proof reading. Using this free service, authors can make their results available to the community, in citable form, before we publish the edited article. We will replace this Accepted Manuscript with the edited and formatted Advance Article as soon as it is available.

You can find more information about Accepted Manuscripts in the [author guidelines](#).

Please note that technical editing may introduce minor changes to the text and/or graphics, which may alter content. The journal's standard [Terms & Conditions](#) and the ethical guidelines, outlined in our [author and reviewer resource centre](#), still apply. In no event shall the Royal Society of Chemistry be held responsible for any errors or omissions in this Accepted Manuscript or any consequences arising from the use of any information it contains.

Assessment of Magnesium-Based Biomaterials: From Bench to Clinic

View Article Online
DOI: 10.1039/C9BM00289H

Mehdi Razavi^{1,2,*}, Yan Huang¹

¹Brunel Center for Advanced Solidification Technology (BCAST), Institute of Materials and Manufacturing, Brunel University London, Uxbridge, London UB8 3PH, UK

²Department of Radiology, School of Medicine, Stanford University, Palo Alto, California 94304, USA

*Corresponding author: E-mail: merazavi@stanford.edu; mrazavi2659@gmail.com
Tel.: +16504847293.

Table of contentsView Article Online
DOI: 10.1039/C9BM00289H

| | |
|--|----|
| 1. Introduction..... | 4 |
| 2. <i>In vitro</i> corrosion tests | 5 |
| 2.1. Electrochemical corrosion test..... | 5 |
| 2.2. Immersion test..... | 6 |
| 2.2.1. Weight loss | 6 |
| 2.2.2. Hydrogen (H ₂) evolution | 6 |
| 2.2.3. pH monitoring..... | 7 |
| 2.2.4. Mg ion release..... | 8 |
| 2.3. Corrosion fatigue | 8 |
| 2.4. Effect of chemical composition and microstructure | 8 |
| 2.5. Effect of the inorganic and organic contents of the solution | 9 |
| 2.5.1. Inorganic contents..... | 9 |
| 2.5.2. Organic contents | 10 |
| Proteins | 10 |
| Glucose | 11 |
| 2.6. Selection of suitable medium for <i>in vitro</i> corrosion studies | 11 |
| 2.7. Buffer-regulated corrosion..... | 12 |
| 2.8. Flow rate of solution..... | 13 |
| 2.9. Effect of temperature | 13 |
| 3. <i>In vivo</i> corrosion measurement | 13 |
| 4. Post corrosion analysis..... | 14 |
| 4.1. Corrosion morphology..... | 14 |
| 4.2. Corrosion products..... | 14 |
| 5. Corrosion rate measurement | 15 |
| 6. Type of corrosion..... | 16 |
| 7. Corrosion mechanism | 16 |
| 8. Multifunctional <i>in vivo</i> corrosion characterization system (CCS)..... | 18 |
| 9. Transdermal sensing of H ₂ | 18 |
| 10. Computed Tomography (CT) | 19 |
| 11. Angiography and Intravascular ultrasound (IVUS)..... | 20 |
| 12. Histology..... | 20 |
| 13. Clinical follow-up..... | 21 |
| 14. Summary | 21 |
| References..... | 22 |

Abbreviations

Open Circuit Potential: OCP

Electrochemical Impedance Spectroscopy: EIS

Corrosion Potential: E_{corr}

Corrosion Current Density: I_{corr}

Scanning Rate: SR

Corrosion Rate: CR

Simulated Body Fluid: SBF

Inductively coupled plasma-atomic emission spectrometer: ICP-AES

Dulbecco's Modified Eagle Medium: DMEM

Minimum Essential Medium: MEM

Scanning Electron Microscope: SEM

Corrosion Characterization System: CCS

Hounsfield Units: HU

Intravascular ultrasound: IVUS

Tumor Necrosis Factor Alpha: TNF- α

Osteonecrosis in the Femoral Head: ONFH

Abstract

View Article Online
DOI: 10.1039/C9BM00289H

Despite the high potential of biodegradable magnesium (Mg) alloys as a new generation of biomaterials for orthopaedic and cardiovascular implantation, their high corrosion rate in body fluid limits their suitability for clinical applications. Extensive research has been performed to improve the corrosion resistance of Mg-based biomaterials. Researchers have also been working to develop new testing and assessment techniques to evaluate the corrosion performance and other *in vitro* and *in vivo* properties of their modified Mg alloys. The objective of this review is to present the principles and operation procedures of commonly used standard methods for assessment of Mg-based biomaterials from bench to clinic. The pros and cons of each of these methods are discussed, together with factors for consideration to choose the right methodology. This review also presents the current state and challenges in understanding the testing of Mg-based biomaterials.

Keywords: Mg-based biomaterials; Testing; *In vitro*; *In vivo*; Clinic.

1. Introduction

Current research has shown the potential of biodegradable Mg alloys as a new class of metallic biomaterials¹⁻⁴. Mg implants can be dissolved, absorbed and/or excreted, so that implant removal surgery is not required⁵⁻⁷. However, one major concern with Mg is its high corrosion rate, making it unpredictable in the physiological environment^{8,9,10}. In fact, Mg is electrochemically very active, with a standard potential of -2.7 V (Mg/Mg²⁺, standard hydrogen potential)¹¹. Fast corrosion, results in implant failure before a bone fracture is healed. Bone healing process normally takes over 3 months while currently available biodegradable Mg alloys cannot maintain their mechanical integrity within this time frame¹². Another problem is about corrosion products of Mg, i.e. hydrogen gas (H₂) bubbles which form around the implant¹³⁻¹⁶. The H₂ bubbles evolved from a corroding Mg implant can be accumulated in the form of gas pockets in the tissues surrounding the implant, which may ultimately lead to the separation of tissue layers and tissue necrosis^{17,18}. In a worst-case scenario, patient death is possible if a large amount of H₂ bubbles diffuse through the blood circulating system and block blood stream. Decreasing the corrosion rate of Mg alloys is the only way to solve the problem. At a decreased corrosion rate, Mg²⁺ ions, H₂ bubbles and OH⁻ ions will be produced more slowly, allowing the host tissue to gradually adjust or deal with the biodegradation products^{17,19,20}. Extensive research has been done to decrease the Mg's corrosion rate, including new alloy development²¹, reinforcing with bioceramic particles²², thermomechanical processing²³ and coating them with biopolymers²⁴ and/or bioceramics²⁵ using different coating techniques such as electrodeposition²⁶, electrophoretic deposition²⁷ and dip-coating²⁸ (**Figure 1**).

Figure 1

In the development of a new Mg-based biomaterial, testing and assessment becomes therefore critically important to evaluate the efficacy of these modifications. Corrosion of Mg alloys for example is a complex process and its complete characterization demands a good combination of a range of methodologies²⁹. Probably, an *in vitro* corrosion system suitable for Mg alloys should be established³⁰. However, it is important to understand the current methods and select the right test with proper experimental conditions, before a perfect system is in position³¹. The aim of this review is to therefore describe in detail commonly used methods for assessing the performance of Mg to clarify the applicability, benefits and disadvantages associated with individual methods and the key points which should be considered during the test. Hopefully,

this review provides guidelines for investigators who work in the field of Mg-based biomaterials and broader metallic biomaterials. View Article Online
DOI: 10.1039/C9BM00289H

2. *In vitro* corrosion tests

2.1. Electrochemical corrosion test

Most of the studies on surface modifications of Mg-based biomaterials set anticorrosion as the prime objective³². Electrochemical corrosion test is a convenient way to assess the corrosion rate by monitoring the open circuit potential (OCP), polarization and electrochemical impedance spectroscopy (EIS) using a three-electrode system including reference, counter and working electrodes^{27,33}. Following are some aspects that affect the corrosion results during the electrochemical corrosion tests.

As the most popular and easiest test, potentiodynamic polarization is used by researchers to provide data of corrosion potential (E_{corr}) and corrosion current density (I_{corr})^{31,34}. One key parameter in potentiodynamic polarization test is scanning rate (SR). I_{corr} rises and zero current potential shifts to more negative value by an increase in SR. Because electrode system at a low SR is in or close to a steady-state and electron transfer rate is equal to electron consumption rate at this state, an accurate zero current potential can be acquired. As SR increases, the steady state is disturbed, and the electron transfer rate becomes more than the electron consumption rate in cathode reaction, which results in the gathering of electrons on the electrode surface and causes a negative shift of zero current potential. However, a lower SR gives a clearer current density peak. Hence, SR should be slow enough and is recommended to be 0.5 or 1 mV/s^{31,33}.

It should be considered that the common Mg alloys do not exhibit a uniform corrosion mode due to the presence of second phases such as intermetallics or filler particles. The conversion of I_{corr} to a corrosion rate (CR) can only be carried out if uniform corrosion is assumed³⁵. Hence, potentiodynamic polarization test results do not usually produce an accurate CR for Mg. Running OCP before starting the test is important for stabilizing sample surface with the solution. When a metal surface is exposed to an electrolyte solution, it takes a certain amount of time to form an electrical double layer on the surface and then to be stabilized³⁶. For Mg alloys, OCP time is about 15-20 min. Another factor is the selection of potential range which provides sufficient information to allow a Tafel-type analysis. In general for Mg alloys -150 to + 500 mV vs OCP is a suitable potential range^{4,31,37,38}.

EIS is a method for surface characterization using the frequency response of AC polarization³⁹. A range of low magnitude polarizing voltages is applied in EIS while resistance and capacitance values are recorded for each frequency. These values can then be utilized to interpret a number of surface properties of the material³¹. The frequency range has an important effect on spectra. It is essential to select frequency range based on the activity of the electrode system. The frequency range of 100 kHz–10 mHz is commonly used for Mg alloys^{40–43}. The lowest frequency is 10 mHz, below which potential noise interference becomes serious. The highest frequency is 100 kHz because EIS data may change due to phase shift from the potentiostat in the higher frequency region⁴⁴. EIS can give data of the surface impedance of a subject to polarization. This is directly related to the corrosion resistance and inversely related to the corrosion rate^{4,31}. By applying an amplitude excitation signal, its response depends on the electrode kinetic processes which normally include several different sub-processes such as charge transfer and mass transfer. By analysing the responses, individual processes may be deduced^{45,46}. Deep understanding of the corrosion process can be obtained by combining the results of EIS and potentiodynamic polarization tests. Following immersion test in the simulated body fluid (SBF), a corroded layer forms, and two capacitive loops are observed at

high frequency and low frequency regions, respectively, in the Nyquist plot at the initial times of immersion, which are due to charge transfer, influence of corrosion products layer and mass transfer⁴⁶. This impedance variation is related to the protection of the corroded layer. In Mg alloys (for example AZ91), the α -phase matrix and γ -phase intermetallics form galvanic couples, and an intense corrosion tend to start at α/γ interfaces. The existence of the inductive loop in EIS spectra is therefore due to this microgalvanic corrosion between the α matrix and γ phase⁴⁷.

2.2. Immersion test

Immersion test according to ASTM G31-72⁴⁸ is commonly used for corrosion assessment of biodegradable Mg alloys. In an immersion test, the progress of corrosion damage can be measured as a function of immersion time in a corrosive environment. In this method, the immersed samples are corroded in the SBF solution, normally at 37°C, and mass loss, mass gain, hydrogen evolution, pH variation, Mg ion release and the corrosion products are determined by a series of techniques, the details of which will be described in following sections. The immersion time and solution volume to surface area ratio (V/S) are the important factors determining the results. A minimum V/S is recommended to be 20 mL/cm². At this ratio, the solution volume is enough to avoid any significant change in response to exhaustion of corrosive constituents, accumulation of corrosion products and pH change as corrosion takes place during the test. However, various ratios of V/S have been reported to be used^{30,49–52}, from 0.33⁵³ to 500 mL/cm²⁵⁴ without justification and the accuracy of the results is questionable. Yang and co-workers³⁰ have assessed the effect of V/S ratio on the corrosion rate by choosing different V/S ratios from 0.67 to 66.7 mL/cm². Their results confirmed that V/S ratio did affect the corrosion rate of Mg alloys and low V/S ratios resulted in higher pH values and reduced corrosion rate, whereas the effect was insignificant at high V/S ratios. According to the implantation area of Mg implants, it is suggested to study both high and low V/S ratios to simulate the *in vivo* corrosion properties of Mg bone screws in a bone marrow cavity and Mg plates and screws in cortical bone or muscle tissues, respectively³³.

2.2.1. Weight loss

To measure weight loss, a sample with known weight is placed in the SBF for pre-determined times and then cleaned with chromic acid (CrO₃) to remove the corrosion products formed on the surface before weight measurement^{55,56}. The difference between starting and final weights is the weight loss^{57,58}. Weight gain is measured before surface corrosion products are removed. Usually, a mixture of CrO₃ and AgNO₃ is utilized to efficiently clean the corrosion products by dissolving Mg(OH)₂^{31,59–61}.

2.2.2. Hydrogen (H₂) evolution

Oversaturated H₂ in blood and tissues tends to be collected in tissue cavities, forming H₂ gas pockets^{15,62}. The gas cavity interacts rapidly with the surrounding tissue⁶³ and induces mechanical disturbance to bone, leading to the formation of callus⁶⁴. H₂ evolution is the main reason for which Mg was abandoned in its early medical applications^{2,65,66}. H₂ evolution reflects corrosion kinetics and can be utilized to estimate the corrosion rate of Mg alloys. Assessing the corrosion rate of Mg alloys by measuring H₂ evolution rate is useful and important. This is because 1) H₂ release is a damaging process for Mg implantation and needs to be monitored; 2) the mole value of evolved H₂ is exactly equal to that of the dissolved Mg and therefore H₂ evolution rate can give an accurate measurement of Mg corrosion rate; 3) 1 mole of the evolved H₂ is equivalent to 2 moles of OH⁻ produced in the solution and so H₂ evolution rate shows the alkalization rate occurring in the solution⁶⁷. Hence, measuring H₂

evolution has been used as an important technique to compare the biodegradability of different Mg alloys. View Article Online
DOI: 10.1039/C9BM00289H

To measure H₂ evolution, a sample is immersed in the SBF and a collector is placed in the SBF above the sample to collect the H₂ gas once released. According to **Reaction 1** and **Eq. 1**, 1 mol of H₂ gas (22.4 L) directly corresponds to the dissolution of 1 mol of Mg (24.31 g)³¹:



$$PV = nRT \quad \text{(Eq. 1)}$$

where P is standard atmospheric pressure (Pa), V is volume of H₂ (m³), n is the amount of the gas (mol), T is the temperature (K).

According to the volume of H₂ and **Eq. 1**, the corrosion rate can be calculated by considering 1 mL H₂ = 0.001083 g Mg into **Eq. 2**³³:

$$\text{CR} = W/Atp \quad \text{(Eq. 2)}$$

where CR is corrosion rate, W is the weight loss of Mg, A is the surface area of Mg exposed to the corrosive medium, t is exposure time and ρ is density. Consequently, the measurement of H₂ is equivalent to the measurement of weight loss where one atom of Mg produces one H₂ gas molecule.

An H₂ evolution rate of 0.01 ml/cm²/day has been introduced as a tolerated level which can be used for selecting a biomedical Mg alloys as a candidate for further *in vivo* experiments¹⁷.

The diffusion and solubility coefficients of H₂ in different tissues have been widely studied⁶⁸. The solubility of H₂ in tissues depends on the content of proteins, lipids, salinity and the diffusion coefficient of H₂ has a direct correlation with water fraction of the tissue⁶⁸. This might explain why different H₂ evolution rate are seen for Mg alloys in different anatomical implantation sites^{15,69–71}. Accordingly, the local blood flow and the water content of the tissue surrounding implant should be considered for designing biodegradable Mg implants⁷².

2.2.3. pH monitoring

In a non-buffered media, corrosion of Mg can lead to high alkalinity of the electrolyte i.e. pH10–12^{73,74}, and even in buffered solutions, pH increase happens⁷⁵. In the corrosion reactions, cathodic reactions occur and cause this change in the pH value. For some non-bio applications of Mg alloys, the alkaline pH shift on the surface is helpful, because it aids to passivate the Mg surface by forming passive Mg(OH)₂ surface layers. For example, Mg alloys can present a good corrosion performance under atmospheric exposure, where thin electrolyte layers on the alloy surfaces allow strong alkalization⁷⁶. However, such effects are harmful for biological applications. Some Mg corrosion products have also been indicated to have antimicrobial properties, and these corrosion products are formed due to strong pH increase⁷⁷. The pH value obtained in *in vitro* experiments is different from that in *in vivo* experiments since *in vivo* is highly dynamic⁷⁶. On implantation, the pH value of tissues around the implant may reduce to 5, and then increase to 7.4 few weeks post-implantation⁷⁶. As Mg corrodes, OH⁻ is released and enhances the local surface pH to around 12. pH monitoring is normally done from surface or close to the surface of the sample. However, such measured pH value may not be representative of the pH at the sample surface and may be different by several pH units⁷⁸.

This matter should be considered in experiments. pH value is recognised to possess a significant impact on Mg corrosion as increasing pH value can result in the formation of a thick corrosion layer and therefore a reduction in corrosion rate⁷⁹. Accordingly, the maintenance of a particular pH range as it happens naturally *in vivo*, by using a buffer is important⁸⁰, which is practically done through pH monitoring and solution renew or modification^{4,31}.

2.2.4. Mg ion release

Evaluation of released Mg ion in the solution is another method to measure the corrosion rate of biodegradable Mg alloys. Inductively coupled plasma-atomic emission spectrometer is used for this purpose to determine the Mg ion concentration in the solution. Mg ion concentration is converted to corrosion rate according to Eq. 3⁸¹:

$$CR = iV/At \quad (\text{Eq. 3})$$

where CR is corrosion rate, i is Mg ion concentration, V is solution volume and A is the original surface area exposed to the corrosive media and t is the immersion time. This technique has the same problem as weight loss method, which may have error if the deposited corrosion products cannot be entirely cleaned from the sample surface.

2.3. Corrosion fatigue

Implants in bone and blood vessel applications are usually used under cyclic loading conditions such as alterations between compression, tension and bending. Fatigue failure occurs at a cyclic load below the fatigue limit⁸². Combination of electrochemical corrosion and cyclic mechanical loading causes corrosion fatigue, and finally implant failure^{83,84}. The corrosion fatigue of Mg alloys has been studied in 3.5 wt.% NaCl (pH ~ 5)⁸⁵, 5 wt.% NaCl (pH ~ 6.59)⁸⁶ and 0.1N Na₂B₄O₇ (pH ~ 9.3) solutions⁸⁵, but there are no reports regarding the corrosion fatigue of biodegradable Mg alloys in a physiological environment. However, Gu et al⁸⁷ studied the corrosion fatigue behaviours of a die-cast AZ91D Mg alloy and an extruded WE43 Mg alloy in the SBF. Under cyclic loading, both alloys showed increased corrosion rates. This effect was further enhanced with increasing cyclic loading. The corrosion fatigue strength of the AZ91D alloy in the SBF was much lower than that in air, being 20 MPa at 10⁶ cycles whereas the corrosion fatigue strength of the WE43 alloy in SBF was 40 MPa at 10⁷ cycles.

Table 1 summarizes an outline of different *in vitro* corrosion tests and some recommended technical points for experimental designs.

Table 1.

2.4. Effect of chemical composition and microstructure

Careful selection of alloying elements is the first step in designing Mg alloys. A range of alloying elements such as Al, Zn, Ca, Ag, Ce, and Th can be added to improve mechanical properties by microstructural refinement, solid solution hardening and precipitation hardening⁸⁸⁻⁹¹. On the other hand, alloying elements that have electrochemical potentials similar to that of Mg (-2.37 V), such as Y (-2.37V), Nd (-2.43 V) and Ce (-2.48V), and those have relatively high solid solubility in Mg, such as Sc (25.9 wt.% limit), Gd (23.5 wt.% limit) and Dy (25.3 wt.% limit) can decrease corrosion rate by reducing internal galvanic corrosion in physiological environments^{59,92,93}. Among alloying elements, Ca acts as a grain-refining agent in Mg alloys, can stabilize grain size at levels up to 0.5% of the Mg alloy content⁹⁴, and is also an essential element for bone cell signalling and beneficial to bone healing⁹⁵. Zn is one of the most abundant essential nutrients in the human body⁹⁶ and is an effective strengthening element

through both solid solution hardening and precipitation hardening⁹⁷. In terms of corrosion behaviour, the degradability of Mg₁₇Al₁₂ second-phase, tested in SBF using electrochemical measurements, has been found to be lower than that of bare Mg⁹⁸. However, the effect of second-phase particles is complicated, depending on their size, morphology, volume fraction and distribution, in addition to their electrochemical properties. Alloying elements having relatively high solid solubility in Mg, such as Y (12 wt.% limit), Sc (25.9 wt.% limit), Gd (23.5 wt.% limit), and Dy (25.3 wt.% limit) also play a role of solid solution hardening⁸⁹. Nevertheless, it is always of fundamental importance to assure that the amount of alloying elements should be controlled within the safety range in terms of biocompatibility and cytotoxicity.

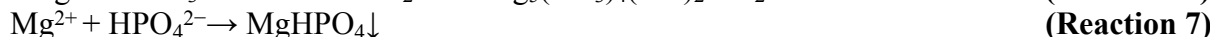
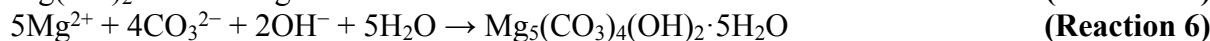
The effect of grain size on material strength is clear and it follows in general the famous Hall-Petch relationship⁹⁹, i.e., yield strength increases with decreasing grain size. Grain size has been shown for some alloys to have a strong impact on the corrosion rate^{100,101}. However, the general effect of grain size on corrosion resistance is not straightforward. The relative dissolution or passivation of a surface has been linked to the total grain boundary length, which is considered a proxy for overall surface reactivity and diffusivity and is normally expressed by the average grain size. Depending on the material and environment combinations, decreased grain size can either increase or decrease the corrosion rate. Corrosion rate is controlled by the diffusion of the reactants through the surface film and grain size particularly can influence this diffusion-controlled process. It has been shown that in an environment where the reaction is favourable for the formation of a surface passivation film, a fine grain microstructure tends to promote the development of a more uniform and tough surface film^{67,100,102}. One of the explanations is that a fine-grained microstructure most likely provides a means for relieving tensile or compression stresses in the surface film by producing porosity through vacancy supply via grain boundaries, thus reducing the tendency of film cracking¹⁰². However, once the aggressive anion concentration exceeds a certain limit, or the reaction favours the dissolution of the surface film when the environment's pH value is low, the film loses its corrosion protection ability^{67,103}. Under this circumstance, the high density of defects and high diffusion rate provided by the grain boundaries will assist the corrosion attack¹⁰⁴. Decreased grain size thus leads to an increasing corrosion rate. More detailed discussion is beyond the scope of this paper but readers are suggested to be careful with observations on corrosions associated with grain size change.

2.5. Effect of the inorganic and organic contents of the solution

2.5.1. Inorganic contents

Blood plasma is a neutral solution contain inorganic contents such as Cl⁻, HPO₄⁻², HCO₃⁻, Mg²⁺, Ca²⁺¹⁰⁵, and organic contents such as amino acids, proteins and glucose^{78,106}. Previous investigations^{44,107,108} have proved that Cl⁻ ions can cause pitting corrosion while phosphates⁴⁴ reduce corrosion rate. Although carbonate¹⁰⁹ can promote corrosion, it can also lead to rapid surface passivation because of magnesium carbonate deposition. In terms of general corrosion, sulphate¹¹⁰ is more aggressive than chloride. Xin and co-workers⁴⁴ have studied the effect of ions in the physiological environment on the corrosion behaviour of a biodegradable Mg alloy. They found that OH⁻ can increase the localized corrosion but stabilize the corrosion products; however, Mg(OH)₂ is a loose layer and not able to provide enough protection. Moreover, Cl⁻ ions on the surface can convert the Mg(OH)₂ layer into soluble MgCl₂ while HCO₃⁻ and HPO₄²⁻

can convert $\text{Mg}(\text{OH})_2$ into more stable $\text{Mg}_5(\text{CO}_3)_4(\text{OH})_2 \cdot 5\text{H}_2\text{O}$ and $\text{Mg}_3(\text{PO}_4)_2$, respectively. The effect of inorganic contents on the corrosion of Mg alloys is as follow (**Reactions 2-7**):³³



The corrosive medium of body fluid consists of a 0.9% NaCl solution with small amounts of other inorganic ions including Ca^{2+} , PO_4^{3-} and HCO_3^- ¹¹¹. Due to the existence of high concentration of Cl^- ions, the physiological environment is highly corrosive for Mg alloys. Other ions may affect corrosion behaviour, either as accelerators or inhibitors. Although Mg^{2+} ions can react with phosphate ions and result in surface layers which protect the surface from corrosion⁷⁶, the precipitation of $\text{Mg}_3(\text{PO}_4)_2$ consumes OH^- , promotes the forward reaction, and accelerate the corrosion of Mg⁴⁷. The dissolution of $\text{Mg}(\text{OH})_2$ by Cl^- makes the surface more active or decreases the protected area, therefore giving rise to further corrosion of Mg. Carbonates can increase or decrease corrosion rate, depending on HCO_3^- concentration. If HCO_3^- concentration exceeds 40 mg/L, the corrosion rate increases because of the accelerated dissolution of the $\text{Mg}(\text{OH})_2$ and MgO protection films. Otherwise, the corrosion is reduced⁴⁵. Since the concentration of HCO_3^- in the SBF is around 256 mg/L¹¹², much higher than 40 mg/L, the carbonates accelerate corrosion rate in the SBF. Sulphates are also corrosive to the Mg but not as much as Cl^- ions¹¹³.

2.5.2. Organic contents

Proteins

Protein adsorption on Mg surface has a significant effect on corrosion rate reduction, since it makes a dense insoluble salt layer, which protects Mg against corrosion⁷⁸. Blood plasma contains around 6.3–8 wt.% of proteins⁷⁸. Zeng et al.¹¹⁴ have shown that adding bovine serum albumin changes OCP to a more positive value in SBF and reduces the localized corrosion. Corrosion behaviour of Mg alloys has also been explored with corrosion media containing proteins^{40,72,115,116}. Proteins such as albumin form a corrosion barrier layer enriched by calcium phosphates on Mg alloys *in vitro* and *in vivo*^{69,117,118} which gives protection against corrosion. Yang et al.¹¹⁹ reported that proteins delay corrosion and alter ion composition of the media. A recent study has shown that adding proteins or corrosion testing in fetal bovine serum decreases the corrosion rate of Mg alloys by 10 to 1000%¹⁴. Corrosion inhibition by albumin addition has also been reported for an AZ91 Mg alloy in SBF solution¹¹⁷, as well as for Mg–Ca alloys in water and in NaCl solutions¹²⁰. These examples show that albumin is effective on enhancing corrosion resistance for Mg and its alloys, although this effect can be strongly alloy dependent⁷⁶. Generally, protein adsorption layers act as a protective layer between the metal surface and the corrosive media, thus inhibiting corrosion. Proteins may also complex with the metal ions and accelerate corrosion; such effects would be expected to depend on the type of metal. Adsorption of albumin happens on the surface of Mg. However, the nature of the protein adsorption layer can change with time due to Mg corrosion, which is time dependent. For example, a pH increase on Mg surface can cause denaturation or desorption of proteins. Experiments with serum addition in the SBF solution have also been performed showing the time-dependent complex behaviour¹²¹. For Mg–Ca alloys, serum proteins accelerated corrosion and for AZ31 Mg alloy, the serum proteins enhanced the corrosion rate in first 3 days immersion and then decreased it, whereas for AZ91 Mg alloy a decreased corrosion rate was

noticed. Yamamoto and Hiromoto have assessed the effect of amino acids and proteins on the corrosion behaviour of pure Mg⁷⁸ and amino acids were found to increase Mg corrosion, which was explained by the chelating effect of Mg cations. However, serum proteins reduced the corrosion. Hence, proteins play a key role on the corrosion behaviour of Mg alloys and the effect of proteins can change with corrosion time. Thus tests in different time-scales may cause very different results. To date, very little surface analytical work has been performed to observe the impact of proteins on the nature of the corrosion product layers formed on the Mg alloy surfaces. Clearly, more research on the mechanisms of protein's effect on the corrosion of Mg alloys and on their corrosion product formation is required⁷⁶.

Glucose

It is still challenging for Mg alloys to be implanted in diabetic patients with high levels of blood glucose. So far, the effect of glucose on corrosion of Mg has not yet been clarified. In a research regarding the effect of glucose on the corrosion behaviour of Mg, pure Mg has been demonstrated to have different corrosion behaviours with different glucose contents of saline and Hank's solutions. On one hand, the corrosion of pure Mg accelerates with glucose concentration in saline solutions. As glucose quickly transforms into gluconic acid, which attacks metal oxides and reduces the pH value of the medium, it also encourages the absorption of Cl⁻ ions on the Mg surface and so increases the corrosion rate. On the other hand, for Hank's solutions with higher glucose content, better corrosion resistance has been observed. It can be due to the fact that glucose coordinates Ca²⁺ ions in Hank's solution and therefore improves the formation of Ca-P compounds on the surface of Mg¹⁰⁶. Thus, glucose increases the corrosion rate of pure Mg in saline solution while decreases the corrosion rate of pure Mg in Hank's solution because of the effect of Ca²⁺ and phosphate ions in the Hank's solution, showing medium dependency of glucose effect. The effect of inorganic and organic contents on the corrosion rate of biodegradable Mg alloys has been summarized in **Table 2**.

Table 2.

2.6. Selection of suitable medium for *in vitro* corrosion studies

An important step in *in vitro* experiments of biodegradable Mg alloys is the selection of a suitable test medium. Different types of media that mimic the composition of body fluids have been used in *in vitro* studies such as 0.9 wt.% NaCl solution, SBF, Hanks' solution, DMEM, and PBS^{14,47,79}. The ionic composition of the solutions and concentrations of the buffering agents are different^{4,122}. Mg alloys present different corrosion responses in different solutions. For example, the Icorr for AZ91D Mg alloy obtained in 0.9% NaCl aqueous solution (tested by Yao et al.¹²³) and in Hank's solution (tested by Song et al.⁴¹) was 22.5 μA/cm² and 297 μA/cm², respectively. The difference is substantial. Both inorganic and organic contents have impact on corrosion behaviour, so composition of the solution must be carefully selected. For *in vitro* corrosion tests, a buffer medium containing similar components to blood plasma needs to be used³³. HCO₃⁻ and HPO₄²⁻ change the corrosion behaviour of Mg, because they cause the formation of insoluble corrosion products on the surface which retard the corrosion process. In addition, Mg corrosion releases OH⁻ which interact with buffering agents in the solutions and alters corrosion rate. Therefore, the concentration of buffering agents will also influence the corrosion rate of Mg alloys^{4,122}. For example, in the case where the concentrations of inorganic ions are similar, the buffering concentrations in c-SBF and Hanks' solution are different. It has been shown that the corrosion rate in c-SBF is about one order of magnitude more than that in Hanks' solution. This difference is mostly due to the high concentration of Tris-HCl, which can react with OH⁻, and then accelerates the corrosion of Mg^{4,122}. Even with the same concentration of buffering agents, the type of buffering agents affects the corrosion behaviour

of Mg alloys. Although Hanks' solution contains inorganic ions with concentrations similar to those in the body fluid, the lower concentration of buffering agents and much lower concentration of HCO_3^- ($\sim 4.0 \text{ mmol L}^{-1}$) has a negative effect on *in vitro* corrosion rates. Among SBF solutions such as c-SBF, modified SBF and r-SBF, r-SBF has the same amounts of inorganic ions, buffering agents and HCO_3^- as the body fluids, and therefore it is recommended as an appropriate solution for *in vitro* corrosion for Mg alloys. However, it should be noted that r-SBF does not have amino acids, proteins, and glucose, which means that corrosion performance obtained is accurately the same as that in a body fluid. DMEM contains both organic and inorganic components but with variable contents. DMEM with concentrations of inorganic ions, buffering agents and HCO_3^- equal to those of the body fluid is most appropriate for the *in vitro* corrosion tests of Mg alloys^{4,122}. The Minimum Essential Medium (MEM) is also used as a tissue culture media, which is more realistic than the dilute chloride or Hank's solutions and is closer to the physiological conditions because it has a variety of amino acids and vitamins (in addition to salts) that are present in blood plasma¹⁴. A careful attention needs to be paid to temperature control during test¹⁴. Besides the mentioned inorganic and organic contents of body fluids, cells are another factor affecting the corrosion behaviour of metallic materials inside human body. Macrophages and active oxygen species produced by them have increased the corrosion of Ti¹²⁴. Not only the biological contents but also the biomechanical environment including blood flow may affect Mg corrosion inside body. Based on these discussions, a continuous or controlled flow system¹¹⁸ is desirable for the *in vitro* corrosion assessment for Mg alloys⁷⁸.

2.7. Buffer-regulated corrosion

To maintain a stable pH level which is critical for the normal function of proteins and cells, the body uses a natural buffer system by the oxidation of organic molecules to create bicarbonate ions that provide the buffer capacity¹²⁵. To reduce pH variations during *in vitro* tests, a pH buffering system is therefore needed. Without buffering, the solution pH level quickly increases and reaches to a level above the pH value that is acceptable for the physiological environment. To limit this pH change without using buffers, one has to either regularly renew the corrosion medium or use a large medium V/S. Therefore, it is more convenient and cost effective to use a buffer system¹²⁶. The commonly used buffering agents in SBF solutions are HEPES, Tris-HCl and HCO_3^- . HEPES and Tris-HCl are buffers which can only consume the produced OH^- during the Mg corrosion. HCO_3^- ($\sim 27 \text{ mmol L}^{-1}$ in the body fluids) as a well-known buffering agent in the body is not only capable of consuming OH^- , but also induces the formation of insoluble carbonates. This will result in different corrosion behaviours in solutions with the same total buffering agent concentration but different HCO_3^- concentrations¹²². NaHCO_3 is also an important buffering system in a cell culture medium by combining H_2CO_3 derived from dissolved CO_2 in the incubator. However, K_{sp} of MgCO_3 in water is 6.82×10^{-6} which is low¹²⁷ and therefore MgCO_3 may precipitate in a medium contain $\text{NaCl} + \text{NaHCO}_3$. In the case of atmospheric corrosion, which contains only 0.3 vol.% of CO_2 , MgCO_3 and its hydrates are formed on the surface of Mg alloys¹²⁸. Typically, 2.2 g/l of NaHCO_3 is added to the SBF solution that is kept in a 5–10% CO_2 atmosphere. The $\text{NaHCO}_3/\text{CO}_2$ system is effective to keep the pH balance in a physiological range and is usually utilized in the cell culture¹²⁶. As another pH buffering system, zwitterion has both positive and negative charges, and has both acid and base. The most common type of zwitterion is HEPES¹²⁹ and it can be used with no special environment requirement (e.g. CO_2 atmosphere). Selection of buffer plays an important role in the corrosion rate control of Mg. According to the studies by Kirkland and co-workers⁸⁰, the weight loss of Mg in the presence of HEPES was 4 times more than that in $\text{NaHCO}_3/\text{CO}_2$ buffer system. For both buffers, corrosion in the MEM solutions was higher, which shows that the presence of amino acids leads to more rapid corrosion of Mg. A possible

reason for the reduced corrosion in $\text{NaHCO}_3/\text{CO}_2$ buffered media is the deposition of a calcium carbonate or magnesium carbonate layer on the surface. Moreover, $\text{NaHCO}_3/\text{CO}_2$ buffer helps the nucleation of CaP on the Mg surface, which cause a lower corrosion rate.

2.8. Flow rate of solution

In vitro immersion tests can be carried out at a static or dynamic state. In static immersion test, samples are immersed in still solution, whereas in a dynamic state, the solution is flowing. Most research has been performed in the static state. Some results indicate that static state does not represent *in vivo* corrosion¹³⁰. Thus, dynamic equipment has been developed for better simulation of the *in vivo* environment. For cardiovascular stents, a Chandler-Loop^{131,132} has been used to simulate the dynamic corrosion of Mg alloys in human blood. A dynamic condition using human blood or modified SBF solutions, with control of rotation speed is recommended for assessing blood contacting devices such as Mg-based cardiovascular stents¹³³. Hiromoto et al.¹³³ have explored the corrosion procedure of pure Mg in 0.6% NaCl under rotational speeds of 1, 120, 1440 r/min and found that solution flow increases Mg corrosion rate by decreasing the formation of corrosion products on the surface. Thus, the flow rate of the solution should be adjusted to be similar to the flow rate of blood in the implanted area. **Figure 2** shows an example of a dynamic corrosion test⁸¹. The amplitude of medium shear stress also affects Mg corrosion behaviour. A low stress protects the surface from localized corrosion while a high stress causes localized corrosion¹¹⁸.

Figure 2.

2.9. Effect of temperature

The body temperature (i.e. 37 °C) increases the corrosion rate and can change the corrosion mechanism and kinetics of corrosion reactions when compared to room temperature. The formation of Ca-phosphates on implant surfaces also depends on temperature⁷⁶. The corrosion rates measured at 37 °C have been reported to be over 100% higher than those measured at 20 °C i.e. There is a twofold increase in the corrosion rate from room temperature to 37 °C. A further 50% increase has been reported when testing at 40 °C, with only a temperature increase of 3 °C. Therefore, strict control of testing temperature around 37°C is strongly recommended^{4,14}.

3. *In vivo* corrosion measurement

The results obtained from *in vitro* studies are usually not reflective of *in vivo* environments, presenting a challenge for researchers^{130,134}. Total amount of body fluid affects the corrosion rate of Mg. The fact that an increased amount of body fluid increases Mg corrosion rate suggests that Mg implantation in a small animal is not always a suitable way to predict the corrosion behaviour of Mg alloys in human body⁷⁸. Witte et al.¹³⁰ found that the corrosion rate *in vivo* is around four orders of magnitude lesser than that of the *in vitro* by a comparison between the *in vitro* and *in vivo* corrosion rate of Mg alloys. The results of this research recommend that the present ASTM standard for *in vitro* corrosion studies cannot be used to present the *in vivo* corrosion rates of Mg alloys. For example, *in vitro* and *in vivo* corrosion experiments on the LAE442 and AZ91D Mg alloys indicated opposite corrosion rates. An AZ91D alloy was found to reduce corrosion rate more than LAE442 *in vitro* while the AZ91D exhibited higher corrosion rate than LAE442 *in vivo*. However, both Mg alloys showed an *in vivo* corrosion rates that were four orders of magnitudes less than those obtained *in vitro*. Evaluation of *in vivo* corrosion particularly in hard tissues is difficult. The blood flow around an implant and some other parameters including oxygen supply, pH value and flow of corrosive media will affect *in vivo* corrosion. A pH value drop for example occurs post-surgery, leading

to a short-term increase in corrosion rate and then creation of a stable corrosion layer. The corrosion process is expected to decrease due to this corrosion layer. Moreover, a lesser content of chloride pitting ions is present *in vivo* in contrast to the *in vitro* in which it is higher. This might explain the overall lower corrosion rates *in vivo*, which is confirmed by the observation of smoother surfaces of implanted samples¹³⁰. Besides, *in vivo* corrosion rate strongly depends on the location of implant because differences in blood flow, the amount of water and ion contents, cells, etc. change with location and affect corrosion behaviour¹³⁵. For example, intramedullary implants displayed more corrosion than subcutaneous implants¹³⁶. Therefore, selecting a proper corrosive media is important and can better simulate an *in vivo* corrosion condition. For example, Walker et al.¹³⁴ immersed Mg, AZ31, Mg-0.8Ca, Mg-1Zn, Mg-1Mn, Mg-1.34Ca-3Zn Mg alloys in Earle's balanced salt solution, MEM, or MEM-containing bovine serum albumin for 1, 2, and 3 weeks. The *in vitro* results, compared with *in vivo* implants in a subcutaneous environment in rats for same time points suggested that, the Earle's balanced salt solution buffered with sodium bicarbonate gives a corrosion rate comparable to those seen *in vivo*. However, the addition of components such as HEPES, vitamins, amino acids, and albumin increased the corrosion rates.

4. Post corrosion analysis

4.1. Corrosion morphology

The corrosion morphology of samples is usually observed under the optical microscope and scanning electron microscope (SEM) before and after cleaning the corrosion products from the Mg surfaces by chromic acid solution^{58,137}. The usual corrosion characteristic of Mg alloys is localised corrosion due to microstructural and chemical heterogeneity and changes from alloy to alloy¹⁴. The surface morphology of Mg changes during the corrosion process starting from formation of microcracks to deposition and growth of corrosion products (**Figure 3**)¹³⁸.

Figure 3.

4.2. Corrosion products

Corrosion of biodegradable Mg alloys is accompanied by the formation of four components including 1) a corroded surface on the implant; 2) released Mg ions and other alloying elements; 3) a large amount of OH⁻; and 4) H₂ gas. Corrosive media used in *in vitro* experiments such as SBF, DMEM and PBS have large amounts of buffering agents such as HCO₃⁻, HPO₄²⁻, Tris-HCl and HEPES, which can consume the produced OH⁻ and mediate immediate variations in the pH values. Thus, although quick corrosion of Mg occurs in these buffered solutions, the pH value changes gradually. The dissolved Mg ends up in two places - the solution and the surface layer. For example, after immersion of pure Mg in the SBF solution for 10 days, more than half of the released Mg ions deposited on the surface layer¹³⁹. The composition of formed corrosion products layer after corrosion changes with the type of solution and the composition of alloys. In SBF solution, Hanks' solution and DMEM with HCO₃⁻ and HPO₄²⁻ ions, insoluble phosphates and carbonates are often formed in the corrosion product layer besides the MgO and/or Mg(OH)₂¹²². Due to the amorphous nature of corrosion products, it is hard to recognize the exact phases that have formed^{11,140}, although, some reports have indicated the formation of crystalline phosphates and carbonates in the layer^{30,140,141}. The main corrosion products in the PBS solution, are magnesium phosphates and Mg(OH)₂. However, insoluble carbonates are also found on samples exposed to PBS, probably formed by the dissolved CO₂ in the solution. The calcium-containing corrosion products on the AZ91 Mg alloy exposed to SBF solution and DMEM tend to aggregate at isolated regions. The high concentration of Cl⁻ ions can change the formed Mg(OH)₂ layer into soluble MgCl₂. This Mg(OH)₂ breakdown reduces the protected area, therefore accelerates the corrosion of the substrate¹²². The corrosion product removal

after immersion is important. Some researchers^{130,142,143} rinse the samples by distilled water and weigh them, others¹⁴⁴ try to remove the corrosion products by brush while others^{54,145,146} clean the samples by 180 g/L chromic acid. These cleaning processes all have some weaknesses: 1) brushing may destroy the matrix of the metals and leave scratches on the surface, which adds to the weight loss, 2) washing by distilled water cannot clean all the corrosion products from the surface, causing weight gain¹³⁰, and 3) washing by chemicals should be paid much attention to avoiding the reactions between the substrate and the chemicals through long-time washing. Furthermore, surface coated samples should avoid chemical cleaning to avoid reactions between the surface and chemicals^{4,33,122}.

5. Corrosion rate measurement

Corrosion rates measured from different experimental method vary and, in complex media which simulate body fluids, measuring corrosion rate accurately is more difficult. Thus, some researchers measure corrosion rate by measuring the volume of H₂ gas which releases from Mg during corrosion. This method has some restrictions especially because of the variations of atmospheric pressure and possible H₂ leakages from the experimental set-up^{29,72}. The most common methods to measure corrosion rate *in vitro* are gravimetric measurements (weight loss) and electrochemical tests (polarization and EIS). In polarization test, I_{corr} is calculated by Tafel extrapolation to the cathodic and anodic regions of the curves. Then, I_{corr} is converted to the corrosion rate based on Faraday's Laws (**Eq. 4**)¹³⁰:

$$CR = tMI_{\text{corr}} / nF\rho \quad (\text{Eq. 4})$$

where CR is the corrosion rate, t is the exposure time, I_{corr} is the corrosion current density, M is the Molar mass, n is the number of electrons involved in the corrosion reaction, F is the Faraday's constant (96 485 As/mol), ρ is the standard density of Mg alloy¹³⁰. Also, the corrosion rate (Pi (mm/year)) can be calculated from I_{corr} (mA/cm²) according to **Eq. 5**^{137,147}:

$$Pi = 22.85I_{\text{corr}} \quad (\text{Eq. 5})$$

Note that, electrochemical test is a kind of accelerating corrosion process, which cannot simulate the real corrosion situation *in vivo*, but can be utilized as a basic method of measuring corrosion properties³³. In the weight loss method, the corrosion rate is calculated according to **Eq. 6**^{56,122}:

$$CR = W/At \quad (\text{Eq. 6})$$

where CR is the corrosion rate, W is the weight loss of the sample, A is exposure area and t is exposure time in the solution. Before weighing, the sample is usually immersed in chromic acid for around 5–10 min to clean the corrosion products¹²². The corrosion rate (C (mg/cm²/day)) can be converted to an average corrosion rate (PW (mm/year)) using **Eq. 7**^{148,149}:

$$PW = 2.10C \quad (\text{Eq. 7})$$

The Mg corrosion reactions indicate that 1 mol (i.e. 24.31 g) of Mg metal corrodes and produces 1 mol (22.4 L) of H₂ gas. Consequently, the H₂ release rate (VH (ml/cm²/day)) can be related to the weight loss (ΔW (mg/cm²/day)) by **Eq. 8**^{11,150,151}:

$$\Delta W = 1.085VH \quad (\text{Eq. 8})$$

And, the corresponding corrosion rate, PH (mm/year), is calculated using **Eq. 9**¹³⁷:

$$PH = 2.279VH \quad (\text{Eq. 9})$$

In the case of Mg corrosion, there is a good agreement^{11,147} between the measured corrosion rate by the weight loss rate and that evaluated from the H₂ release rate.

Corrosion rate can also be evaluated from implant volume change using three-dimensional (3D) imaging data. Assuming a homogeneous alloy, the implant volume decrease can be converted to the corrosion rate by modifying Eq. 6 with the weight loss (W) substituted by the reduction in volume (ΔV) as **Eq. 10**¹³⁰:

$$CR = \Delta V / At \quad (\text{Eq. 10})$$

where CR is the corrosion rate, ΔV is the reduction in volume that is equal to the remaining implant volume subtracted from the initial implant volume, A is the surface area of implant exposed to corrosive media and t is the exposure time¹³⁰. The corrosion rate equations and relevant parameters are summarized in **Table 3**.

Table 3.

6. Type of corrosion

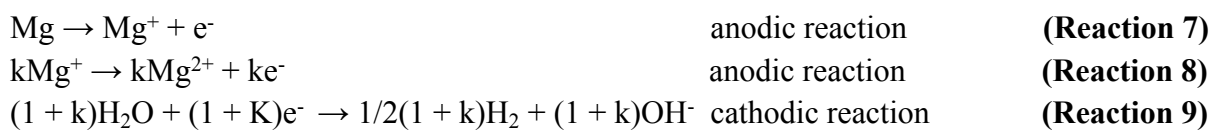
Another aspect of corrosion of Mg alloys is that Mg alloys usually are not corroded in a uniform manner. Generally, non-uniform corrosion is seen, as either the surface of material or the surroundings indicate heterogeneities. Most Mg alloys are of multi-phases and grain structures and therefore chemically and microstructurally heterogeneous. The existence of second-phase particles (intermetallic) is usually desired for enhancing mechanical properties. Even for pure Mg, owing to limited solubility, most impurities in Mg are present as particles or inclusions. Since basically all alloying elements and impurities are nobler than Mg, intermetallic phases, rich of alloying elements, will naturally act as local cathodes coupled with the Mg matrix as the anode. In all cases of galvanic corrosion, the coupling efficiency depends on the potential difference of the anodic and cathodic regions. Thus, alloying elements or impurities with a low overpotential for H₂ release reaction are more harmful for Mg than the alloying elements with a higher overpotential for H₂ release. Coupling with nobler surface sites not only increases the corrosion of the Mg matrix, but also results in a non-uniform corrosion morphology. A non-uniform corrosion process can be risky, particularly when under mechanical loads; the mechanical stability may be locally lost and implant is fractured from that site. Furthermore, life-time prediction is more difficult for non-uniform corrosion compared to uniform corrosion⁷⁶. Overall, pitting and localized corrosion are the most common corrosion mechanisms of Mg alloys in the physiological environment, which are related to not only the heterogeneous structure of the alloy, but also the compositions of the solution. For example, AZ91 Mg alloy has a much high tendency to pitting corrosion when exposed to the SBF solution¹²².

7. Corrosion mechanism

The corrosion mechanisms of Mg alloys in an aqueous solution is mainly determined by the electrochemical reaction with water to generate Mg(OH)₂ and H₂ (**Figure 4**). Although the overall corrosion behaviour of Mg alloys has not yet been studied systematically, it is assumed that corrosion reactions of Mg alloys are in principle similar to those of pure Mg. The main corrosion product of Mg alloys is Mg(OH)₂ in both *in vitro* and *in vivo* environments⁹⁵.

Mg(OH)₂ is stable in the range of pH values of 8.5–11, depending on the concentration of Mg²⁺ in the solution, but soluble in the neutral or acidic range of pH values. As corrosion progresses, the pH value of the medium near the Mg surface will rise with the accumulation of OH⁻. This causes formation of the Mg(OH)₂ on the surface because the solubility of Mg(OH)₂ reduces with the increase of OH⁻ concentration because of the increase in the pH value of the solution. The accumulated Mg(OH)₂ layer on the surface of Mg can act as a protective layer against the corrosion by inhibiting mass diffusion between the Mg substrate and the solution. The Mg²⁺ ion release continuously decreases in initial days of immersion, indicating that maturing and thickening of accumulated Mg(OH)₂ layer has contributed to the reduction of Mg²⁺ release⁷⁸.

Corrosion reaction converts Mg to Mg²⁺ in two electrochemical steps, involving the uni-positive ion, Mg⁺, as a short-life intermediate, as given by reactions (7) and (8) and the anodic partial reactions are balanced by the cathodic partial reaction of H₂ release, reaction (9)¹³⁷:



The uni-positive ion, Mg⁺, is reactive and has a life time too short to be detected¹¹, and can react chemically with water. Therefore, a fraction, k, of the uni-positive Mg⁺, reacts electrochemically according to reaction (8) to Mg²⁺, and the complement reacts chemically according to reaction (10)¹³⁷:



The overall reaction is as below (reaction (11)):



The corrosion of Mg is partly electrochemical, and electrochemical measurements would be thus expected to predict a corrosion rate lower than the real value as measured by weight loss or hydrogen evolution tests. The apparent electrochemical valence is given by (1 + k). The standard electrode potential of Mg²⁺/Mg is -2.37 V at 25 °C, while the actual corrosion potential of Mg is typically -1.7 V in dilute chloride media. Song et al.¹¹³ reported that the existence of Cl⁻ ions increases the electrochemical reaction rate via MgCl₂ formation, which hydrolyses to create HCl in a localized auto-catalytic process. During the corrosion process, a high amount of Mg ions dissolves into the test solution and the pH value enhances as a result of reaction (9). High speed release of Mg ion reduces the formation of calcium phosphate. Therefore, the increase in pH value plays an important role in calcium phosphate formation. In the SBF solution, insoluble magnesium phosphate (Mg₃(PO₄)₂), may also form as corrosion products according to reaction (12)¹⁵²:



As discussed above, due to reaction (9) the pH value of SBF solution increases. Consumption of OH⁻ by H₃PO₄ accelerates reaction (10) and encourages the formation of insoluble Mg₃(PO₄)₂, which is the reason for the low Ca/P ratio in the corrosion products. The corrosion product layer has been found to contain calcium phosphate, magnesium carbonate and hydroxyapatite. It has been suggested that the layer is formed by the interaction of Mg ions

with calcium, carbonate and phosphate ions, which are constituents of Hank's and SBF solutions, by the following precipitation reactions (reaction (13) and (14))¹⁵³:



Li et al.¹³⁹ have indicated that the pH value of SBF solution in contact with pure Mg increases initially and then becomes stable after around 3 days due to a balance between the formation and dissolution of the corrosion products. This is the reason for the detection of similar weight percentage of elements in the corrosion products after 7 days immersion.

Following the cathodic reaction (reaction (9)), OH⁻ releases into the solution. This can enhance the localized pH value, increase the precipitation and stabilization of the corrosion products and thereby pitting corrosion is gradually reduced. Chemical dissolution together with the electrolyte penetration result in the corrosion on the surface of Mg alloy, leading to the formation of corrosion products, such as magnesium hydroxide and magnesium phosphate, as discussed above. However, it is hard for the corrosion products to form in the microcathode (γ phase) area of Mg alloy where H₂ is released. The corrosion products precipitate generally at the vicinity of the microanode (α phase) due to the OH⁻ diffusion⁴⁶. Accordingly, the active point decreases and passivation by the corrosion products layer enhances with time. As previously mentioned, due to microstructural heterogeneity, pitting corrosion occurs in the Mg alloy. For example, in the case of AZ91 Mg alloy, γ (Mg₁₇Al₁₂) secondary phase has a higher standard voltage and forms an electrolysis junction with the α -matrix. Pits are usually formed because of the selective attack along the γ phase⁴⁷. The corrosion product can reduce this galvanic effect between the two phases⁴⁶. In long-term immersion tests, the galvanic effect decreases, and the mechanism of corrosion changes from general to pitting corrosion. For Mg, the critical chloride concentration which is needed for pitting corrosion is around 30 mmol/L i.e. much lower than that in SBF which contains 142 mmol/l. Thus, pitting corrosion is a common corrosion type of Mg alloys exposed to the SBF⁴⁷. Petty et al.¹⁵⁴ also showed that the corrosion of a two-phase Mg alloy, in a typical environment like 3% NaCl is characterised by heterogeneous corrosion due to the micro-galvanic coupling with the second phase particle acting as an efficient cathode and accelerating the corrosion of the alpha-Mg matrix. Moreover, filiform corrosion has been seen on (un-coated) Mg¹⁵⁵, Mg–Al¹⁵⁶, Mg–Li¹⁵⁷, Mg–6Zn–1Y–0.6Zr¹⁵⁸, Mg–Zn–Y¹⁵⁹, and Mg–Y¹⁶⁰ in salt solutions.

Figure 4

8. Multifunctional in vivo corrosion characterization system (CCS)

A CCS has been recently developed by Doepke et al¹⁶¹. CCS allows real-time monitoring of corrosion products in the solution such as OH⁻, Mg²⁺, and H₂ during immersion tests (i.e. commonly used corrosion products to study the corrosion of Mg alloys). This system also records EIS simultaneously in the same solution. This kind of approaches give a better understanding of the dynamics of the corrosion process in real-time during immersion tests, rather than providing a corrosion rate at the end of the immersion tests (Figure 5a-d).

9. Transdermal sensing of H₂

The remarkably rapid transport of H₂ through skin enables the measurement of H₂ concentration transdermally at the surface of the skin above a biodegrading Mg sample implanted subcutaneously in mice. Although the concentrations are very low (ca. 30–400 μM),

the electrochemical H₂ biosensor has adequate limit of detection to easily measure these levels. Measurements are rapid, taking about 30s for the biosensor to reach a steady reading. Measured H₂ levels correlate with the corrosion rates as determined by weight loss of explanted samples after being implanted¹⁶². Hence, H₂ sensing shows promise as an effective means for monitoring the biodegradation of Mg alloys *in vivo*. H₂ sensing has advantages over traditional techniques of monitoring biodegradation rate such as weight loss of explanted samples, X-ray measurements, and μ -CT. Compared to weight loss, it gives a measure of biodegradation rate at the time of measurement rather than integrated over the entire time of implantation. Compared to X-ray and μ -CT, the instrumentation is much less expensive and involves no exposure to radiation. Additionally, *in vivo* H₂ sensing has numerous benefits compared to sensing the other corrosion products such as OH⁻ and Mg²⁺. First, only H₂ has the possibility of being monitored non-invasively due to its high permeability through skin⁶³. This is a significant advantage compared to the surgical insertion of a biosensor as would be the case for pH or Mg²⁺. Second, no significant background level of H₂ exists in mammals that needs to be corrected for. For example, the concentration of H₂ in mouse blood is only ca. 1 Mm¹⁶³. Background level is an issue with Mg²⁺ where a relatively high concentration exists *in vivo* (Mg²⁺ concentration in adult serum is 0.75–0.95 mM). A biosensor for Mg²⁺ would need to have sufficient precision to detect small increases due to biodegradation above this substantial background. Also, the commonly used electrochemical sensor for Mg²⁺, an ion-selective electrode, suffers serious interference from Ca²⁺, which exists *in vivo* at a higher concentration (ca. 2.0–2.6 mM in adult serum). Third, H₂ is relatively nonreactive in biological media, making it a robust biodegradation marker¹⁶⁴. By comparison, released OH⁻ will be consumed by buffer, which severely compromises the measurement of pH for monitoring biodegradation. Furthermore, Mg²⁺ reacts with various anions such as OH⁻ and carbonate to form precipitates and with naturally occurring organic ligands (such as lactate and citrate) and proteins to form complexes that might obscure it from a sensor such as an ion-selective electrode¹⁶⁵. Fourth, a commercially available electrochemical H₂ sensor with excellent limit of detection and selectivity already exists⁶³.

However, the main fundamental limitation of sensing H₂ transdermally is the maximum tissue depth from implant to skin surface that the H₂ can permeate through to produce a sufficiently high concentration for detection by pressing the sensor tip to the skin. Thus, this technique might not be applicable to deep implants such as on the thigh bone where permeation through a thick muscle layer would be necessary. The applicability would also be expected to vary among animals because of physical differences. Practical considerations include the need for periodic calibration of the sensor with H₂ standards at appropriate intervals to ensure that measurements are accurate. In addition, the membrane permeability of the H₂ microsensor changes with time, causing loss in sensitivity of as much as 50% over several months¹⁶². This new technique is noninvasive, fast and requires no major equipment (**Figure 5e-h**).

Figure 5

10. Computed Tomography (CT)

CT is an imaging modality for bone which is based on the attenuation of x-rays by the object's features, measured in Hounsfield Units (HU). Air has a HU value of -1000 and water has a value of 0. The range HU of human bone is in the range of 250 to 3000¹⁶⁶. μ CT is used for small biological and non-biological samples for which a very high resolution is needed. Metallic orthopaedic implants such as screws, can distort the CT images due to their ferromagnetic properties. Both titanium alloy and stainless steel implants can be imaged with CT, however the resolution of titanium is better and there is less signal interference^{167,168}.

Unlike traditional metallic biomaterials such as stainless steel and titanium, Mg creates minimal interference and is visible by CT without any artifacts¹⁶⁶. μ CT is performed at different time points, for example 1 week, 4 weeks and 12 weeks after the implantation using following parameters at 70 kV voltage, 500 μ A current, and 1000 ms exposure time¹⁶⁹. For example, Myrissa et al¹⁶⁹ have used cylindrical pins with 1.6 mm diameter and 8 mm length made of pure Mg, Mg2Ag and Mg10Gd for implantation into the bone. The μ CT images of pure Mg shows gas bubbles formation in the intramedullary cavity at week 1 post-implantation. New bone formation around the pin can also be seen with μ CT. In the μ CT images of the Mg10Gd implants, at 12 weeks post-implantation, pins have been broken and completely reduced to small pieces surrounded by newly formed bone (**Figure 6**). Hence, gas formation due to the release of H₂ bubbles, new bone formation and degradation or fracture of Mg implants can be imaged using μ CT.

Figure 6

11. Angiography and Intravascular ultrasound (IVUS)

In vivo angiography is used to investigate the safety and efficacy of the biodegradable stents. The angiography images can show the existence of thrombogenesis, as well as in-stent restenosis in the Mg-based stents. However, the results are needed to be compared with a control group such 316L stainless steel stents, to demonstrate that whether the biodegradable Mg-based stents are safe and efficient *in vivo* or not. The follow-up IVUS is used to evaluate the expansion level, initial hyperplasia degree and the occurrences of thrombosis of stents in different implantation periods. The stents need to be completely expanded and well apposed to the vessel wall with no sign of elastic recoil and fracture, reflecting excellent radial strength and compliance of the stent. Furthermore, a thin layer of endothelium if appeared on the surface of the stent struts, can be imaged using IVUS. For example, Mao et al¹⁷⁰ used a Mg alloy Mg-2.2Nd-0.1Zn-0.4Zr (denoted as JDBM-2) stent. They implanted JDBM-2 into rabbits for long-term evaluation. They have assessed biodegradability, biocompatibility, structural and mechanical integrity of the stent *in vivo* using angiography and IVUS for 6 months (**Figure 7**).

Figure 7

12. Histology

When animals are sacrificed at the end of study, Mg implants surrounded by their tissues are harvested for histological studies. The aim of doing histology is to see the interaction of implant with the surrounded tissue. Using histological images, the bone density and bone implant contact area can be calculated. For this purposes, usually Haemotoxylin and Eosin staining is enough, however, inflammation around the implant can be further stained and analysed using inflammatory markers such as tumor necrosis factor alpha (TNF- α). In addition, for detection of signs of inflammatory response around the implants, the presence of inflammatory cells such as neutrophils, monocytes, macrophages, or multinucleated giant cells and also increase in the number of osteoclasts are tested. For example Schaller et al¹⁷¹ implanted a biodegradable Mg plate/screw osteosynthesis systems on the frontal bone of adult miniature pigs to evaluate the tissue response of the WE43 Mg alloy with and without a plasma electrolytic surface coating. Using histological analyses, they showed significantly lower corrosion rates and increased bone density and bone implant contact area around the coated screws compared to the uncoated screws (**Figure 8**).

Figure 8

13. Clinical follow-up

In recent years, the rapid advancement in metallurgy field has enabled scientists and engineers to fabricate Mg-based biomaterials with much higher corrosion resistance and improved mechanical properties, which inspired more surgeons to reconsider the potential of biodegradable Mg alloys for clinical applications¹⁷². Mg or its alloys based orthopaedic devices or implants have been tested to fix fractures or bone flaps^{173–175}. For example Zhao et al¹⁷³ conducted surgeries in patients suffering from association of research circulation osseous stage II/III osteonecrosis in the femoral head (ONFH) using specifically designed high purity Mg screws to fix vascularized bone flaps. Within the 12-month follow up-period using radiographic imaging, patients treated with Mg screws fixation showed significantly higher satisfactory therapeutic results in the Harris hip score and bone flap displacement. This was the very first clinical trial and greatly contributed to the acceleration of product registration process of pure Mg-based screws for its application in ONFH reconstruction surgery. These promising treatment outcomes encouraged Dr. Zhao's team to develop innovative surgical protocols for patients with different bone fracture indications, including fixation with Mg screws for femoral neck fracture, metatarsal fracture, diaphyseal defect, acetabular defect, and femoral head fracture (**Figure 9**)¹⁷².

Figure 9

Clinical follow-up is usually performed at 1, 4, 8, 12, 24 weeks and 1 year following implantation of Mg. X-ray and low-dose radiation CT are performed to evaluate the bone healing process and determine the volume of formed H₂ bubbles. In a clinical study, Kim et al¹⁷⁶ assessed gas formation and other biological effects of a biodegradable Mg alloy. They worked on the Mg-5Ca screws with an outer diameter of 2.0 mm, inner diameter of 1.6 mm, and length of 10.0 mm. Their study was performed on patients 20 years or older having metatarsal or midfoot fractures requiring internal fixation. All patients had bony union at 3 months and after 6 months, the metatarsal fracture was completely healed with a small radiolucent area in the screw insertion site. In fact, foot anteroposterior and oblique X-ray images showed a radiolucent lesion on metatarsal neck fractures meaning gas formation by Mg screw (red arrows), which has decreased over time. The diameter of the inserted Mg screw also significantly reduced overtime meaning biodegradation of Mg implants. Axial, coronal, and sagittal CT scans also show multiple air bubbles surrounding Mg screws inserted into metatarsal fracture, which has decreased over time. Especially, postoperative 12 weeks and 6 months CT scans show small amounts of gas in soft tissue as compared to postoperative 1, 4, and 8 weeks (**Figure 10**).

Figure 10

14. Summary

Development of magnesium-based biomaterials will continue to rely on tests to collect initial data. In this review we presented a detailed description of various test methods from *in vitro* to animal studies and clinical trials and outlined advantages and disadvantages of each method. Where necessary, critical technical points for experimental design have also been given. Examples of possible sources of errors have also been discussed in the text. As shown here, various *in vitro* and *in vivo* test methods have been designed to evaluate the corrosion behaviour of Mg alloys as biodegradable implants. All of the experimental techniques discussed in this review are complementary to each other. No single test provides all of the data needed to fully analyse the corrosion performance of Mg alloys. Although these experimental methods provide an in-depth understanding of Mg corrosion behaviour, comparisons between different studies

are difficult because different parameters are often involved in measurement, including solution type, the ratio of exposing surface area to solution volume, temperature of solution and selection of buffers, etc. Besides, current research performs on a large variety of Mg alloys in different simulated physiological environments and using different experimental approaches. It is therefore difficult to have a clear overall picture of Mg alloy corrosion rates as their biomedical application is concerned. Hence, a standard test method needs to be established to describe a unique in vitro, in vivo, and clinical testing and assessment method of Mg-based biomaterials. Since corrosion rate and hydrogen evolution of Mg is so important, having a standard method would be helpful to compare the results of different studies which will facilitate their clinical translation.

Acknowledgement

The authors acknowledge the European Community's Seventh Framework Programme (FP7/2007-2013) under grant agreement no FP7-SME 606112 and MeDe Innovation, the EPSRC Centre for Innovative Manufacturing in Medical Devices [grant number EP/K029592/1] through the EPSRC Fresh Idea Fund.

References

- 1 M. P. Staiger, A. M. Pietak, J. Huadmai and G. Dias, *Biomaterials*, 2006, **27**, 1728–1734.
- 2 F. Witte, *Acta Biomater.*, 2010, **6**, 1680–1692.
- 3 A. Purnama, H. Hermawan, J. Couet and D. Mantovani, *Acta Biomater.*, 2010, **6**, 1800–1807.
- 4 N. T. Kirkland and N. Birbilis, *Magnesium Biomaterials Design, Testing, and Best Practice*, 2014.
- 5 M. Carboneras, M. C. García-Alonso and M. L. Escudero, *Corros. Sci.*, 2011, **53**, 1433–1439.
- 6 P. Gill, *J. Biomater. Nanobiotechnol.*, 2012, **03**, 10–13.
- 7 Y. Huang, D. Liu, L. Anguilano, C. You and M. Chen, *Mater. Sci. Eng. C. Mater. Biol. Appl.*, 2015, **54**, 120–32.
- 8 M. Razavi, M. Fathi, O. Savabi, D. Vashae and L. Tayebi, *Mater. Lett.*, 2015, **155**, 97–101.
- 9 M. Razavi, M. Fathi, O. Savabi and M. Boroni, *Res. Rev. Mater. Sci. Chem.*, 2012, **1**, 15–58.
- 10 M. H. Fathi, M. Meratian and M. Razavi, *J. Biomed. Nanotechnol.*, 2011, **7**, 441–445.
- 11 G. Song and a. Atrens, *Adv. Eng. Mater.*, 2003, **5**, 837–858.
- 12 M. Razavi, M. Fathi, O. Savabi, L. Tayebi and D. Vashae, *J. Mater. Sci. Mater. Med.*, DOI:10.1007/s10856-018-6170-1.
- 13 B. Li, P. Gao, H. Zhang, Z. Guo, Y. Zheng and Y. Han, *Biomater. Sci.*, 2018, **6**, 3202–3218.
- 14 N. T. Kirkland, J. Lespagnol, N. Birbilis and M. P. Staiger, *Corros. Sci.*, 2010, **52**, 287–291.
- 15 F. Witte, V. Kaese, H. Haferkamp, E. Switzer, A. Meyer-Lindenberg, C. J. Wirth and H. Windhagen, *Biomaterials*, 2005, **26**, 3557–3563.
- 16 I. M. Ghayad, M. A. Maamoun, W. A. Metwally, A. N. Abd El-Azim and Z. M. El-Baradie, *Chem. Mater. Res.*, 2015, **7**, 27–41.
- 17 G. Song, *Corros. Sci.*, 2007, **49**, 1696–1701.
- 18 M. Razavi, M. Fathi, O. Savabi, D. Vashae and L. Tayebi, *J. Mater. Sci. Mater. Med.*, 2015, **26**, 1–7.
- 19 J. Li and Y. Huang, in *IOP Conference Series: Materials Science and Engineering*,

- IOP Publishing, 2014, vol. 63, p. 12112.
- 20 Y. Huang, D. B. Liu, M. X. Xia and L. Anguiliano, *Mater. Sci. Forum*, 2013, **765**, 813–817.
- 21 B. Zberg, P. J. Uggowitzer and J. F. Löffler, *Nat. Mater.*, 2009, **8**, 887–891.
- 22 A. Dubey, S. Jaiswal and D. Lahiri, *J. Mater. Eng. Perform.*, 2019, **28**, 800–809.
- 23 N. Sriraman and S. Kumaran, *Mater. Res. Express*, , DOI:10.1088/2053-1591/ab0323.
- 24 C. Wang, Z. Yi, Y. Sheng, L. Tian, L. Qin, T. Ngai and W. Lin, *Mater. Sci. Eng. C*, 2019, **99**, 344–356.
- 25 M. Razavi, M. Fathi, O. Savabi, D. Vashae and L. Tayebi, *J. Biomed. Mater. Res. - Part A*, 2015, **103**, 1798–1808.
- 26 M. Horynová, M. Remešová, L. Klakurková, K. Dvořák, I. Ročňáková, S. Yan, L. Čelko and G. L. Song, *J. Am. Ceram. Soc.*, 2019, **102**, 123–135.
- 27 M. Razavi, M. Fathi, O. Savabi, D. Vashae and L. Tayebi, *Ann. Biomed. Eng.*, 2014, 1–14.
- 28 A. Patil, S. H. Zaky, R. Chong, K. Verdelis and E. Beniash, *J. Biomed. Mater. Res. - Part B Appl. Biomater.*, 2019, **107**, 342–351.
- 29 G. L. Makar and J. Kruger, *Int. Mater. Rev.*, 1993, **38**, 138–153.
- 30 L. Yang and E. Zhang, *Mater. Sci. Eng. C*, 2009, **29**, 1691–1696.
- 31 N. T. Kirkland, N. Birbilis and M. P. Staiger, *Acta Biomater.*, 2012, **8**, 925–936.
- 32 H. Li, F. Peng, D. Wang, Y. Qiao, D. Xu and X. Liu, *Biomater. Sci.*, 2018, **6**, 1846–1858.
- 33 Z. Zhen, T. F. Xi and Y. F. Zheng, *Trans. Nonferrous Met. Soc. China (English Ed.)*, 2013, **23**, 2283–2293.
- 34 M. Razavi, M. Fathi, O. Savabi, D. Vashae and L. Tayebi, *Surf. Eng.*
35 *Astm*, in *Astm G 102*, 1999, vol. 89, pp. 1–7.
- 36 J. Wang, *Analytical Electrochemistry, Third Edition*, 2006.
- 37 N. T. Kirkland, M. P. Staiger, D. Nisbet, C. H. J. Davies and N. Birbilis, *JOM*, 2011, **63**, 28–34.
- 38 M. Razavi, M. Fathi, O. Savabi, D. Vashae and L. Tayebi, *Surf. Interface Anal.*, 2014, **46**, 387–392.
- 39 E. Barsoukov and J. R. Macdonald, *Impedance Spectrosc. Theory, Exp. Appl.*, 2005, 1–595.
- 40 M. B. Kannan and R. K. S. Raman, *Biomaterials*, 2008, **29**, 2306–2314.
- 41 Y. W. Song, D. Y. Shan and E. H. Han, *Mater. Lett.*, 2008, **62**, 3276–3279.
- 42 Y. Xin, J. Jiang, K. Huo, G. Tang, X. Tian and P. K. Chu, *J. Biomed. Mater. Res. Part A*, 2009, **89**, 717–726.
- 43 M. Razavi, M. Fathi, O. Savabi, D. Vashae and L. Tayebi, *Metall. Mater. Trans. A*, 2015, **46**, 1394–1404.
- 44 Y. Xin, K. Huo, H. Tao, G. Tang and P. K. Chu, *Acta Biomater.*, 2008, **4**, 2008–15.
- 45 G. Baril and N. Pébère, *Corros. Sci.*, 2001, **43**, 471–484.
- 46 Y. Zhang, C. Yan, F. Wang and W. Li, *Corros. Sci.*, 2005, **47**, 2816–2831.
- 47 Y. Xin, C. Liu, X. Zhang, G. Tang, X. Tian and P. K. Chu, *J. Mater. Res.*, 2007, **22**, 2004–2011.
- 48 *Astm*, *ASTM Standards: G31-72*, 2012, vol. 72.
- 49 L. Xu, E. Zhang and K. Yang, *J. Mater. Sci. Mater. Med.*, 2009, **20**, 859–867.
- 50 A. C. Hänni, P. Gunde, M. Schinhammer and P. J. Uggowitzer, *Acta Biomater.*, 2009, **5**, 165, 170.
- 51 X. Gu, Y. Zheng, Y. Cheng, S. Zhong and T. Xi, *Biomaterials*, 2009, **30**, 484–498.
- 52 M. Razavi, M. H. Fathi, O. Savabi, D. Vashae and L. Tayebi, *Phys. Sci. Int. J.*, 2014, **4**, 708–722.

- 53 Q. Wang, L. Tan, W. Xu, B. Zhang and K. Yang, *Mater. Sci. Eng. B*, 2011, **176**, 1718–1726. View Article Online
DOI: 10.1059/C9BM00289H
- 54 L. Xu, E. Zhang, D. Yin, S. Zeng and K. Yang, *J. Mater. Sci. Mater. Med.*, 2008, **19**, 1017–1025.
- 55 M. Razavi, *Annu. Res. Rev. Biol.*, 2014, **4**, 3716–3733.
- 56 M. Razavi, M. H. Fathi and M. Meratian, *Mater. Lett.*, 2010, **64**, 2487–2490.
- 57 M. Razavi, M. Fathi, O. Savabi, B. Hashemi Beni, D. Vashae and L. Tayebi, *Colloids Surfaces B Biointerfaces*, 2014, **117**, 432–440.
- 58 O. Savabi, M. Razavi, S. M. Razavi, D. Vashae, M. Fathi, F. Heidari, M. Manshaei and L. Tayebi, *Appl. Surf. Sci.*, 2014, **313**, 60–66.
- 59 N. Hort, Y. Huang, D. Fechner, M. Störmer, C. Blawert, F. Witte, C. Vogt, H. Drücker, R. Willumeit, K. U. Kainer and F. Feyerabend, *Acta Biomater.*, 2010, **6**, 1714–25.
- 60 D. Vojtech, H. Ciova and K. Volenec, *Met. Mater.*, 2006, **44**, 211–223.
- 61 H. Wang, Z. M. Shi and K. Yang, *Adv. Mater. Res.*, 2008, **32**, 207–210.
- 62 F. Witte, J. Fischer, J. Nellesen, C. Vogt, J. Vogt, T. Donath and F. Beckmann, *Acta Biomater.*, 2010, **6**, 1792–1799.
- 63 J. Kuhlmann, I. Bartsch, E. Willbold, S. Schuchardt, O. Holz, N. Hort, D. Höche, W. R. Heineman and F. Witte, *Acta Biomater.*, 2013, **9**, 8714–8721.
- 64 T. Kraus, S. F. Fischerauer, A. C. Hänzi, P. J. Uggowitz, J. F. Löffler and A. M. Weinberg, *Acta Biomater.*, 2012, **8**, 1230–8.
- 65 D. Noviana, D. Paramitha, M. F. Ulum and H. Hermawan, *J. Orthop. Transl.*, 2016, **5**, 9–15.
- 66 M. Razavi, M. Fathi, O. Savabi, S. M. Razavi, F. Heidari, M. Manshaei, D. Vashae and L. Tayebi, *Appl. Surf. Sci.*, 2014, **313**, 60–66.
- 67 G. Song, *Adv. Eng. Mater.*, 2005, **7**, 563–586.
- 68 T. Langø, T. Mørland and a O. Brubakk, *Undersea Hyperb. Med.*, 1996, **23**, 247–272.
- 69 L. Xu, G. Yu, E. Zhang, F. Pan and K. Yang, *J. Biomed. Mater. Res. A*, 2007, **83A**, 703–711.
- 70 F. Witte, H. Ulrich, M. Rudert and E. Willbold, *J. Biomed. Mater. Res. Part A*, 2007, **81**, 748–756.
- 71 R. A. Kaya, H. Cavuşoğlu, C. Tanik, A. A. Kaya, O. Duygulu, Z. Mutlu, E. Zengin and Y. Aydin, *J. Neurosurg. Spine*, 2007, **6**, 141–9.
- 72 F. Witte, N. Hort, C. Vogt, S. Cohen, K. U. Kainer, R. Willumeit and F. Feyerabend, *Curr. Opin. Solid State Mater. Sci.*, 2008, **12**, 63–72.
- 73 J. A. Grogan, B. J. O'Brien, S. B. Leen and P. E. McHugh, *Acta Biomater.*, 2011, **7**, 3523–3533.
- 74 E. Ghali, W. Dietzel and K. U. Kainer, *J. Mater. Eng. Perform.*, 2013, **22**, 2875–2891.
- 75 C. Lorenz, J. G. Brunner, P. Kollmannsberger, L. Jaafar, B. Fabry and S. Virtanen, *Acta Biomater.*, 2009, **5**, 2783–2789.
- 76 S. Virtanen, *Mater. Sci. Eng. B*, 2011, **176**, 1600–1608.
- 77 D. a. Robinson, R. W. Griffith, D. Shechtman, R. B. Evans and M. G. Conzemius, *Acta Biomater.*, 2010, **6**, 1869–1877.
- 78 A. Yamamoto and S. Hiromoto, *Mater. Sci. Eng. C*, 2009, **29**, 1559–1568.
- 79 W. F. Ng, K. Y. Chiu and F. T. Cheng, *Mater. Sci. Eng. C*, 2010, **30**, 898–903.
- 80 N. T. Kirkland, J. Waterman, N. Birbilis, G. Dias, T. B. F. Woodfield, R. M. Hartshorn and M. P. Staiger, *J. Mater. Sci. Mater. Med.*, 2012, **23**, 283–291.
- 81 B. Liu and Y. F. Zheng, *Acta Biomater.*, 2011, **7**, 1407–1420.
- 82 B. a. James and R. a. Sire, *Biomaterials*, 2010, **31**, 181–186.
- 83 C. R. F. Azevedo, *Eng. Fail. Anal.*, 2003, **10**, 153–164.

- 84 E. A. Magnissalis, S. Zinelis, T. Karachalios and G. Hartofilakidis, *J. Biomed. Mater. Res. Part B, Appl. Biomater.*, 2003, **66**, 299–305. View Article Online
DOI: 10.1059/C9BM00289H
- 85 a Eliezer, E. Gutman, E. Abramov and Y. Unigovski, *J. Light Met.*, 2001, **1**, 179–186.
- 86 M. S. Bhuiyan, Y. Mutoh, T. Murai and S. Iwakami, *Int. J. Fatigue*, 2008, **30**, 1756–1765.
- 87 X. N. Gu, W. R. Zhou, Y. F. Zheng, Y. Cheng, S. C. Wei, S. P. Zhong, T. F. Xi and L. J. Chen, *Acta Biomater.*, 2010, **6**, 4605–4613.
- 88 M. Razavi and Y. Huang, *Recent Pat. Nanotechnol.*, , DOI:10.2174/1872210513666181231122808.
- 89 C. Liu, Z. Ren, Y. Xu, S. Pang, X. Zhao and Y. Zhao, *Scanning*, 2018, 2018, 1–15.
- 90 H. Yang, C. Liu, P. Wan, L. Tan and K. Yang, *APL Mater.*, , DOI:10.1063/1.4828935.
- 91 D. Tie, F. Feyerabend, N. Hort, D. Hoeche, K. U. Kainer, R. Willumeit and W. D. Mueller, *Mater. Corros.*, 2014, **65**, 569–576.
- 92 Y. Chen, Z. Xu, C. Smith and J. Sankar, *Acta Biomater.*, 2014, **10**, 4561–4573.
- 93 L. Yang, Y. Huang, F. Feyerabend, R. Willumeit, C. Mendis, K. U. Kainer and N. Hort, *Acta Biomater.*, 2013, **9**, 8499–8508.
- 94 Y. C. Li, M. H. Li, W. Y. Hu, P. D. Hodgson and C. E. Wen, *Mater. Sci. Forum*, 2010, **654–656**, 2192–2195.
- 95 Z. Li, X. Gu, S. Lou and Y. Zheng, *Biomaterials*, 2008, **29**, 1329–1344.
- 96 J. Li, Y. Song, S. Zhang, C. Zhao, F. Zhang, X. Zhang, L. Cao, Q. Fan and T. Tang, *Biomaterials*, 2010, **31**, 5782–5788.
- 97 S. Zhang, X. Zhang, C. Zhao, J. Li, Y. Song, C. Xie, H. Tao, Y. Zhang, Y. He, Y. Jiang and Y. Bian, *Acta Biomater.*, 2010, **6**, 626–640.
- 98 M. B. Kannan, *Mater. Lett.*, 2010, **64**, 739–742.
- 99 N. Hansen, *Scr. Mater.*, 2004, **51**, 801–806.
- 100 C. op't Hoog, N. Birbilis and Y. Estrin, *Adv. Eng. Mater.*, 2008, **10**, 579–582.
- 101 K. D. Ralston, N. Birbilis and C. H. J. Davies, *Scr. Mater.*, 2010, **63**, 1201–1204.
- 102 D. Orlov, K. D. Ralston, N. Birbilis and Y. Estrin, *Acta Mater.*, 2011, **59**, 6176–6186.
- 103 R. Parsons, *Atlas of electrochemical equilibria in aqueous solutions*, 2003, vol. 13.
- 104 D. Song, A. B. Ma, J. H. Jiang, P. H. Lin, D. H. Yang and J. F. Fan, *Corros. Sci.*, 2011, **53**, 362–373.
- 105 R. C. Zeng, Y. Hu, S. K. Guan, H. Z. Cui and E. H. Han, *Corros. Sci.*, 2014, **86**, 171–182.
- 106 R.-C. Zeng, X.-T. Li, S.-Q. Li, F. Zhang and E.-H. Han, *Sci. Rep.*, 2015, **5**, 13026.
- 107 L. Wang, T. Shinohara and B. P. Zhang, *J. Alloys Compd.*, 2010, **496**, 500–507.
- 108 R. Rettig and S. Virtanen, *J. Biomed. Mater. Res. Part A*, 2009, **88**, 359–369.
- 109 Y. Jang, B. Collins, J. Sankar and Y. Yun, *Acta Biomater.*, 2013, **9**, 8761–70.
- 110 L. J. Yang, Y. H. Wei, L. F. Hou and D. Zhang, *Corros. Sci.*, 2010, **52**, 345–351.
- 111 A. Oyane, H.-M. Kim, T. Furuya, T. Kokubo, T. Miyazaki and T. Nakamura, *J. Biomed. Mater. Res. A*, 2003, **65**, 188–195.
- 112 S. B. Cho, K. Nakanishi, T. Kokubo, N. Soga, C. Ohtsuki, T. Nakamura, T. Kitsugi and T. Yamamuro, *J. Am. Ceram. Soc.*, 1995, **78**, 1769–1774.
- 113 G. L. Song and A. Atrens, *Adv. Eng. Mater.*, 1999, **1**, 11–33.
- 114 R. Zeng, W. Dietzel, F. Witte, N. Hort and C. Blawert, *Adv. Eng. Mater.*, 2008, **10**, 3–14.
- 115 W. D. Müller, M. L. Nascimento, M. Zeddies, M. Córscico, L. M. Gassa and M. A. F. L. De Mele, *Mater. Res.*, 2007, **10**, 5–10.
- 116 A. T. Kuwahara H, Al-Abdullat Y, Mazaki N, Tsutsumi S, *Mater. Trans.*, 2001, **42**, 1317–21.

- 117 C. Liu, Yunchang Xin, X. Tian and P. K. Chu, *J. Mater. Res.*, 2007, **22**, 1806–1814.
- 118 J. Lévesque, H. Hermawan, D. Dubé and D. Mantovani, *Acta Biomater.*, 2008, **4**, 284–95.
- 119 L. Yang, N. Hort, R. Willumeit and F. Feyerabend, *Corros. Eng. Sci. Technol.*, 2012, **47**, 335–339.
- 120 C. L. Liu, Y. J. Wang, R. C. Zeng, X. M. Zhang, W. J. Huang and P. K. Chu, *Corros. Sci.*, 2010, **52**, 3341–3347.
- 121 X. N. Gu, Y. F. Zheng and L. J. Chen, *Biomed. Mater.*, 2009, **4**, 065011.
- 122 Y. Xin, T. Hu and P. K. Chu, *Acta Biomater.*, 2011, **7**, 1452–1459.
- 123 Z. Yao, L. Li and Z. Jiang, *Appl. Surf. Sci.*, 2009, **255**, 6724–6728.
- 124 Y. Mu, T. Kobayashi, M. Sumita, a Yamamoto and T. Hanawa, *J. Biomed. Mater. Res.*, 2000, **49**, 238–43.
- 125 J. E. Hall, *Physiology*, 2010, 1091.
- 126 C. D. Helgason and C. Miller, *Basic Cell culture protocols*, 2005, vol. 290.
- 127 D. R. Lide, *Handb. Chem. Phys.*, 2003, **53**, 2616.
- 128 M. Jönsson, D. Persson and D. Thierry, *Corros. Sci.*, 2007, **49**, 1540–1558.
- 129 N. E. Good, G. D. Winget, W. Winter, T. N. Connolly, S. Izawa and R. M. M. Sing, *Biochemistry*, 1966, **5**, 467–477.
- 130 F. Witte, J. Fischer, J. Nellesen, H.-A. Crostack, V. Kaese, A. Pisch, F. Beckmann and H. Windhagen, *Biomaterials*, 2006, **27**, 1013–1018.
- 131 J. Geis-Gerstorfer, C. Schille, E. Schweizer, F. Rupp, L. Scheideler, H. P. Reichel, N. Hort, a Nolte and H. P. Wendel, *Mater. Sci. Eng. B Solid-State Mater. Adv. Technol.*, 2011, **176**, 1761–1766.
- 132 C. Schille, M. Braun, H. P. Wendel, L. Scheideler, N. Hort, H. P. Reichel, E. Schweizer and J. Geis-Gerstorfer, *Mater. Sci. Eng. B Solid-State Mater. Adv. Technol.*, 2011, **176**, 1797–1801.
- 133 S. Hiromoto, A. Yamamoto, N. Maruyama, H. Somekawa and T. Mukai, *Corros. Sci.*, 2008, **50**, 3561–3568.
- 134 J. Walker, S. Shadanbaz, N. T. Kirkland, E. Stace, T. Woodfield, M. P. Staiger and G. J. Dias, *J. Biomed. Mater. Res. - Part B Appl. Biomater.*, 2012, **100 B**, 1134–1141.
- 135 J. Reifenrath, A.-K. Marten, N. Angrisani, R. Eifler and A. Weizbauer, *Biomed. Mater.*, 2015, **10**, 045021.
- 136 E. Willbold, K. Kalla, I. Bartsch, K. Bobe, M. Brauneis, S. Remennik, D. Shechtman, J. Nellesen, W. Tillmann, C. Vogt and F. Witte, *Acta Biomater.*, 2013, **9**, 8509–8517.
- 137 Z. Shi and A. Atrens, *Corros. Sci.*, 2011, **53**, 226–246.
- 138 S. Mostofi, E. B. Rad, H. Wiltsche, U. Fasching, G. Szakacs, C. Ramskogler, S. Srinivasaiah, M. Ueçal, R. Willumeit, A. M. Weinberg and U. Schaefer, *PLoS One*, , DOI:10.1371/journal.pone.0159879.
- 139 L. Li, J. Gao and Y. Wang, *Surf. Coatings Technol.*, 2004, **185**, 92–98.
- 140 R. Rettig and S. Virtanen, *J. Biomed. Mater. Res. A*, 2007, **88**, 359–69.
- 141 M. Razavi, M. Fathi, O. Savabi, B. Hashemi Beni, D. Vashae and L. Tayebi, *Ceram. Int.*, 2014, **40**, 9473–9484.
- 142 S. Zhang, J. Li, Y. Song, C. Zhao, X. Zhang, C. Xie, Y. Zhang, H. Tao, Y. He, Y. Jiang and Y. Bian, *Mater. Sci. Eng. C*, 2009, **29**, 1907–1912.
- 143 Y. Wang, M. Wei and J. Gao, *Mater. Sci. Eng. C*, 2009, **29**, 1311–1316.
- 144 M. Schinhammer, A. C. Hänzi, J. F. Löffler and P. J. Uggowitz, *Acta Biomater.*, 2010, **6**, 1705–1713.
- 145 F. Witte, F. Feyerabend, P. Maier, J. Fischer, M. Störmer, C. Blawert, W. Dietzel and N. Hort, *Biomaterials*, 2007, **28**, 2163–2174.
- 146 E. Zhang, W. He, H. Du and K. Yang, *Mater. Sci. Eng. A*, 2008, **488**, 102–111.

- 147 Z. Shi, M. Liu and A. Atrens, *Corros. Sci.*, 2010, **52**, 579–588.
- 148 S. D. Cramer and B. S. Covino, *Asm*, 2003, **13**, 1135.
- 149 M. Fontana, *McGraw-Hill* 173, 1987, .
- 150 M. C. Zhao, M. Liu, G. L. Song and A. Atrens, *Corros. Sci.*, 2008, **50**, 3168–3178.
- 151 M. C. Zhao, M. Liu, G. Song and A. Atrens, *Corros. Sci.*, 2008, **50**, 1939–1953.
- 152 M. F. Morks, *Mater. Lett.*, 2004, **58**, 3316–3319.
- 153 A. Atrens, M. Liu and N. I. Zainal Abidin, *Mater. Sci. Eng. B Solid-State Mater. Adv. Technol.*, 2011, **176**, 1609–1636.
- 154 R. L. Petty and W. Davidson, *J. Electrochem. Soc.*, 1962, **76**, 363.
- 155 P. Schmutz, V. Guillaumin, R. S. Lillard, J. A. Lillard and G. S. Frankel, *J. Electrochem. Soc.*, 2003, **150**, B99.
- 156 Y. Song, D. Shan, R. Chen and E.-H. Han, *Corros. Sci.*, 2009, **51**, 1087–1094.
- 157 O. Lunder, J. E. Lein, S. M. Hesjevik, T. K. Aune and K. Nisancioglu, *Mater. Corros.*, 1994, **45**, 331–340.
- 158 Y. Song, D. Shan, R. Chen and E. H. Han, *Corros. Sci.*, 2010, **52**, 1830–1837.
- 159 S. Izumi, M. Yamasaki and Y. Kawamura, *Corros. Sci.*, 2009, **51**, 395–402.
- 160 M. Liu, P. Schmutz, P. J. Uggowitz, G. Song and A. Atrens, *Corros. Sci.*, 2010, **52**, 3687–3701.
- 161 A. Doepke, J. Kuhlmann, X. Guo, R. T. Voorhees and W. R. Heineman, *Acta Biomater.*, 2013, **9**, 9211–9219.
- 162 D. Zhao, T. Wang, J. Kuhlmann, Z. Dong, S. Chen, M. Joshi, P. Salunke, V. N. Shanov, D. Hong, P. N. Kumta and W. R. Heineman, *Acta Biomater.*, 2016, **36**, 361–368.
- 163 N. Nakashima-Kamimura, T. Mori, I. Ohsawa, S. Asoh and S. Ohta, *Cancer Chemother. Pharmacol.*, 2009, **64**, 753–761.
- 164 I. Ohsawa, M. Ishikawa, K. Takahashi, M. Watanabe, K. Nishimaki, K. Yamagata, K. I. Katsura, Y. Katayama, S. Asoh and S. Ohta, *Nat. Med.*, 2007, **13**, 688–694.
- 165 C. Blaquiere and G. Berthon, *Inorganica Chim. Acta*, 1987, **135**, 179–189.
- 166 A. F. O. Williams and M. B. A. McCullough, in *ASME International Mechanical Engineering Congress and Exposition, Proceedings (IMECE)*, 2016, p. V014T11A035.
- 167 F. B. Christensen, M. Dalstra, F. Sejling, S. Overgaard and C. Bünger, *Eur. Spine J.*, 2000, **9**, 97–103.
- 168 K. A. Feldman, *J. Foot Ankle Surg.*, 2005, **44**, 455–461.
- 169 A. Myrissa, N. A. Agha, Y. Lu, E. Martinelli, J. Eichler, G. Szakács, C. Kleinhans, R. Willumeit-Römer, U. Schäfer and A. M. Weinberg, *Mater. Sci. Eng. C*, 2016, **61**, 865–874.
- 170 L. Mao, L. Shen, J. Chen, X. Zhang, M. Kwak, Y. Wu, R. Fan, L. Zhang, J. Pei, G. Yuan, C. Song, J. Ge and W. Ding, *Sci. Rep.*, , DOI:10.1038/srep46343.
- 171 B. Schaller, N. Saulacic, T. Imwinkelried, S. Beck, E. W. Y. Liu, J. Gralla, K. Nakahara, W. Hofstetter and T. Iizuka, *J. Cranio-Maxillofacial Surg.*, 2016, **44**, 309–317.
- 172 D. Zhao, F. Witte, F. Lu, J. Wang, J. Li and L. Qin, *Biomaterials*, 2017, **112**, 287–302.
- 173 D. Zhao, S. Huang, F. Lu, B. Wang, L. Yang, L. Qin, K. Yang, Y. Li, W. Li, W. Wang, S. Tian, X. Zhang, W. Gao, Z. Wang, Y. Zhang, X. Xie, J. Wang and J. Li, *Biomaterials*, 2016, **81**, 84–92.
- 174 J.-W. Lee, H.-S. Han, K.-J. Han, J. Park, H. Jeon, M.-R. Ok, H.-K. Seok, J.-P. Ahn, K. E. Lee, D.-H. Lee, S.-J. Yang, S.-Y. Cho, P.-R. Cha, H. Kwon, T.-H. Nam, J. H. Lo Han, H.-J. Rho, K.-S. Lee, Y.-C. Kim and D. Mantovani, *Proc. Natl. Acad. Sci. U. S. A.*, 2016, **113**, 716–21.

- 175 H. Windhagen, K. Radtke, A. Weizbauer, J. Diekmann, Y. Noll, U. Kreimeyer, R. Schavan, C. Stukenborg-Colsman and H. Waizy, *Biomed. Eng. Online*, , DOI:10.1186/1475-925X-12-62. View Article Online
DOI:10.1039/C9BM00289H
- 176 Y. K. Kim, K. B. Lee, S. Y. Kim, K. Bode, Y. S. Jang, T. Y. Kwon, M. H. Jeon and M. H. Lee, *Sci. Technol. Adv. Mater.*, 2018, **19**, 324–335.
- 177 Y. Ding, J. Lin, C. Wen, D. Zhang and Y. Li, *Sci. Rep.*, , DOI:10.1038/srep31990.

Figure captions

Figure 1. A tertiary diagram showing requirement of Mg-based biomaterials in terms of mechanical properties (Ductility > 20%, Strength > 200 MPa), biodegradability (Corrosion rate: 0.1-7 mm/year), and biocompatibility (Inflammation score: 1-2 %); Modification of Mg-based biomaterials to meet these requirements include designing the Mg alloys, reinforcing the Mg alloys with bioceramic particles, thermomechanical processing, and coating them with biopolymers and/or bioceramics using different coating techniques such as electrodeposition, electrophoretic deposition and dip-coating.

Figure 2. A schematic diagram of the dynamic immersion test bench. Hank's solution is circulated in the bench; The wall shear stress is controlled by adjusting the velocity of flow; The temperature is monitored by a detector integrated into the oxygen detector and controlled with a thermostatic waterbath; The pH value is monitored and regulated by adding diluted HCl or NaOH solution; And the dissolved oxygen concentration is monitored by an oxygen detector and controlled by supplying oxygen and nitrogen. Reproduced with permission from ⁸¹, copyright 2011, Elsevier.

Figure 3. Changes in surface morphology of Mg and Mg alloys during corrosion at day 1, 2, 3 and 8 compared to their morphology before corrosion (i.e. day 0). Changes in Mg and Mg alloys surface morphology have been determined by SEM at day 1, 2, 3 and 8 following immersion in DMEM supplemented with 10% FBS. Two regions have been detected during corrosion include brighter grains (arrows A: corrosion products) and darker areas (arrows B: Mg matrix). The formation of corrosion products in the form of crystals (arrows C) have been detected after 3 and 8 days following immersion on the surface of Mg₂Ag and Pure Mg. Scale bars: 100 μm. Reproduced with permission from ¹³⁸, copyright 2016, PLOS.

Figure 4. Schematic model for corrosion process of a biodegradable Mg alloy (Mg-Zr-Sr-Ho): **Stage I:** Hydrogen evolution: Hydrogen evolution initiates at the interface between the Mg alloy and SBF solution due to the attack of components such as cations, organic substances and anions of the SBF solution, and Mg ions are released into the SBF solution so that an MgO/Mg(OH)₂ layer is formed on the Mg surface; **Stage II:** Mg degradation: As prolonged immersion time in SBF solution, some regions of the MgO/Mg(OH)₂ layer convert to Mg²⁺ because of further attack from SBF solution. Consequently, the Mg substrate in these regions is exposed to the medium directly, leading to further degradation. **Stage III:** Interface degradation: As the degradation proceeds, more regions of the MgO/Mg(OH)₂ layer are corroded constantly and more Mg substrates are exposed. Mg²⁺ may pass through the loosened MgO/Mg(OH)₂ layer and form a new MgO/Mg(OH)₂ layer on the exterior surface. Various components can also penetrate the loosened surface and attack the interior Mg substrate, leading to interface degradation between the Mg matrix and the components of the SBF solution beneath the surface layer. **Stage IV:** Degradation shift: The newly formed MgO/Mg(OH)₂ layer cannot resist dissolution. Hence, uniform dissolution occurs, and some regions are inevitably exposed to the SBF solution. The outer MgO/Mg(OH)₂ layer is dissolved continuously and the corrosion extends to the interior Mg substrate and more regions would be exposed to the SBF solution. **Stage V:** Massive degradation: Some corroded residues may fall off the surface of Mg alloys, causing local pits in the Mg substrate and deeper cavities. Accordingly, the Mg matrix will be further attacked due to the galvanic effects and finally the Mg alloys will degrade completely in the SBF, resulting in the massive degradation. Reproduced with permission from ¹⁷⁷, copyright 2016, Nature.

Figure 5. (a) CCS instrumentation and circuit that allows real-time monitoring of pH, Mg and dissolved H₂ with electrochemical sensors while recording EIS and temperature. Block diagram of the corrosion characterization system instrumentation and cell configuration: (1) temperature probe, (2) water hardness sensor, (3) Ag/AgCl reference electrode, (4) Pt solution ground, (5) pH sensor, (6) H₂ sensor, (7) Mg disk in epoxy resin as a working electrode for EIS, (8) Pt auxiliary electrode for EIS, (9) Ag/AgCl reference electrode for EIS, (A, B) preamplifiers. (M1, M2) MeasureNet workstations; Responses of the potentiometric sensors include results of potentiometric sensor monitoring of (b) the pH, (c) the Mg²⁺ concentration and (d) the concentration of dissolved H₂ during corrosion of Mg samples in NaCl, HEPES and HEPES in NaCl; H₂ measurements on an anaesthetized nude mouse with AZ31 implanted subcutaneously 1 week after implantation. (e) Photograph of mouse with measurement points marked and numbered; (f) Instant currents responses corresponding to numbered points in (e); (g) H₂ concentrations measured at each point as determined from a calibration curve. BL is the measurement in air; (h) H₂ concentration monitored weekly during the 8-week study for AZ31. Reproduced with permission from ¹⁶¹, copyright 2013, Elsevier, and ¹⁶², copyright 2016, Elsevier.

Figure 6. μ CT reconstructions (two-dimensional slices) showing the degradation process at 1, 4 and 12 weeks after the implantation of pure Mg, Mg2Ag and Mg10Gd in the femur bone of Sprague–Dawley® rats. Reproduced with permission from ¹⁶⁹, copyright 2016, Elsevier.

Figure 7. The in vivo aortic angiography showing no acute and late thrombogenesis as well as in-stent restenosis in the JDBM-2 Mg alloy and 316L stainless steel stent after stenting for 1 month, 2 months, 4 months and 6 months. The corresponding follow-up IVUS images showing the longitudinal reconstruction of the abdominal aorta after the JDBM-2 Mg alloy and 316L stainless steel stent implantation. Increased lumen patency and vessel size at different implantation period with nearly complete absence of neointimal hyperplasia are seen. Reproduced with permission from ¹⁷⁰, copyright 2017, Nature.

Figure 8. (a) Surgical access of the frontal bone with plate/screw system and (b) evaluation area. The orientation of the plates has been tracked by placing three screws cranially and two screws caudally; (c-d) After sacrifice, histological analysis has been performed on the proximal and distal parts (a1, a8, b1, and b6), as indicated by the dotted lines in the figure, representative histological preparations of a coated (c) and uncoated screw (d) 12 weeks after surgery (scale bar: 1.0 mm); Mean bone implant contact area of titanium, uncoated and coated screws at 12 weeks and 24 weeks post-implantation (*significant difference in titanium compared to both magnesium implants; **significant difference in magnesium-uncoated compared to coated implants). Reproduced with permission from ¹⁷¹, copyright 2016, Elsevier.

Figure 9. The treatment process of femoral head fracture using two Mg screws. (a) The femoral head has been crushed into two parts as shown in the red circle; (b) the broken femoral head has been connected by two Mg screws (red circle); (c) the femoral head has been repaired as shown in the X-ray imaging on the day of surgery, and (d) the femoral head has been well restored at 3 months post-surgery. Reproduced with permission from ¹⁷², copyright 2017, Elsevier.

Figure 10. Gas formation and biological effects of a biodegradable Mg alloy: Foot anteroposterior and oblique X-ray images of gas formation by Mg-5Ca screws with an outer diameter of 2.0 mm, inner diameter of 1.6 mm, and length of 10.0 mm (red arrows), and axial, coronal, and sagittal CT scan images of air bubbles surrounding Mg screw inserted into

metatarsal fracture for 12 months. Foot anteroposterior and oblique X-ray images showing the radiolucent lesion on 3rd and 4th metatarsal neck fractures meaning gas formation by Mg screw (red arrows), which has decreased over time. The diameter of the inserted Mg screw has reduced showing its biodegradability. Axial, coronal, and sagittal CT scans show multiple air bubbles surrounding Mg screws inserted into metatarsal fracture, which has decreased over time. Especially, postoperative 12 weeks and 6 months CT scans show small amounts of gas in soft tissue as compared to postoperative 1, 4, and 8 weeks. Reproduced with permission from ¹⁷⁶, copyright 2018, National Institute for Materials Science in partnership with Taylor & Francis.

View Article Online
DOI: 10.1039/C9BM00289H

Table 1: An outline of the various *in vitro* corrosion tests and recommended technical points for experimental designs.

| <i>In vitro</i> corrosion tests | Recommended technical points | References |
|--------------------------------------|---|------------|
| Polarisation | Scanning Rate (SR): 0.5 or 1 mV/s OCP times: 15 or 20 min Scanning range:-150 to + 500 mV vs. OCP | 33,36,37 |
| EIS | Frequency range: 100 kHz–10 mHz | 40–43 |
| Weight loss | Solution volume to surface area (V/S): 20 mL/cm ² | 48 |
| Hydrogen (H ₂) evolution | H ₂ evolution < 0.01 ml/cm ² /day | 17 |
| pH monitoring | To use a buffer such as HEPES, Tris–HCl and HCO ₃ ⁻ | 78,80,122 |
| Mg ion release | Removal of corrosion products: Using a mixture of CrO ₃ and AgNO ₃ | 81 |

Table 2. The effect of inorganic and organic contents on the corrosion rate (CR) of biodegradable Mg alloys (Increase↑ or decrease↓ in CR has been shown by black rows). View Article Online
DOI: 10.1039/C9BM00289H

| | Inorganic | | | | | Organic | |
|-------------------|-----------------|--------------------------------|-------------------------------|--------------------------------|-----------------|----------|---------|
| | Cl ⁻ | HPO ₄ ⁻² | HCO ₃ ⁻ | HSO ₄ ²⁻ | OH ⁻ | Proteins | Glucose |
| CR↑ | | | | | | | |
| CR↓ | | | | | | | |
| References | 44,107,108 | 44 | 45,112 | 113 | 44 | 78 | 106 |

CR↑ if Mg is in a solution containing HCO₃⁻ > 40 mg/L

CR↓ if Mg is in a solution containing HCO₃⁻ < 40 mg/L

CR↑ if Mg is in glucose containing saline solution

CR↓ if Mg is in glucose containing Hank's solution

Table 3. Corrosion rate equations and relevant parameters.View Article Online
DOI: 10.1039/C9BM00289H

| Corrosion rate equations | parameters | References |
|--------------------------|---|------------|
| $CR = tM_{icorr}/nF\rho$ | CR: corrosion rate t: exposure time M: Molar mass icorr: corrosion current density, n: number of electrons involved in the corrosion reaction F: Faraday's constant (96 485 As/mol) ρ : standard density of Mg alloy | 130 |
| $P_i = 22.85i_{corr}$ | P_i (mm/year): corrosion rate i_{corr} (mA/cm ²): corrosion current density | 137,147 |
| $CR = W/At$ | CR: corrosion rate W: weight loss A: exposure area t: exposure time | 122 |
| $PW = 2.10CR$ | PW (mm/year): corrosion rate CR (mg/cm ² /day): corrosion rate | 148,149 |
| $\Delta W = 1.085VH$ | ΔW (mg/cm ² /day): weight loss VH (ml/cm ² /day): H ₂ release rate | 11,150,151 |
| $PH = 2.279VH$ | PH (mm/year): corrosion rate VH (ml/cm ² /day): H ₂ release rate | 137 |
| $CR = \Delta V/At$ | CR: corrosion rate ΔV : volume change A: exposure area t: exposure time | 130 |

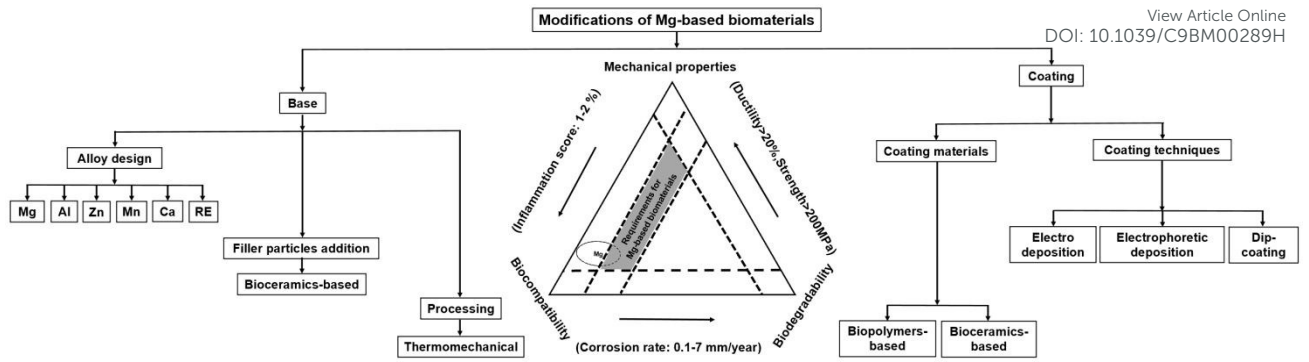
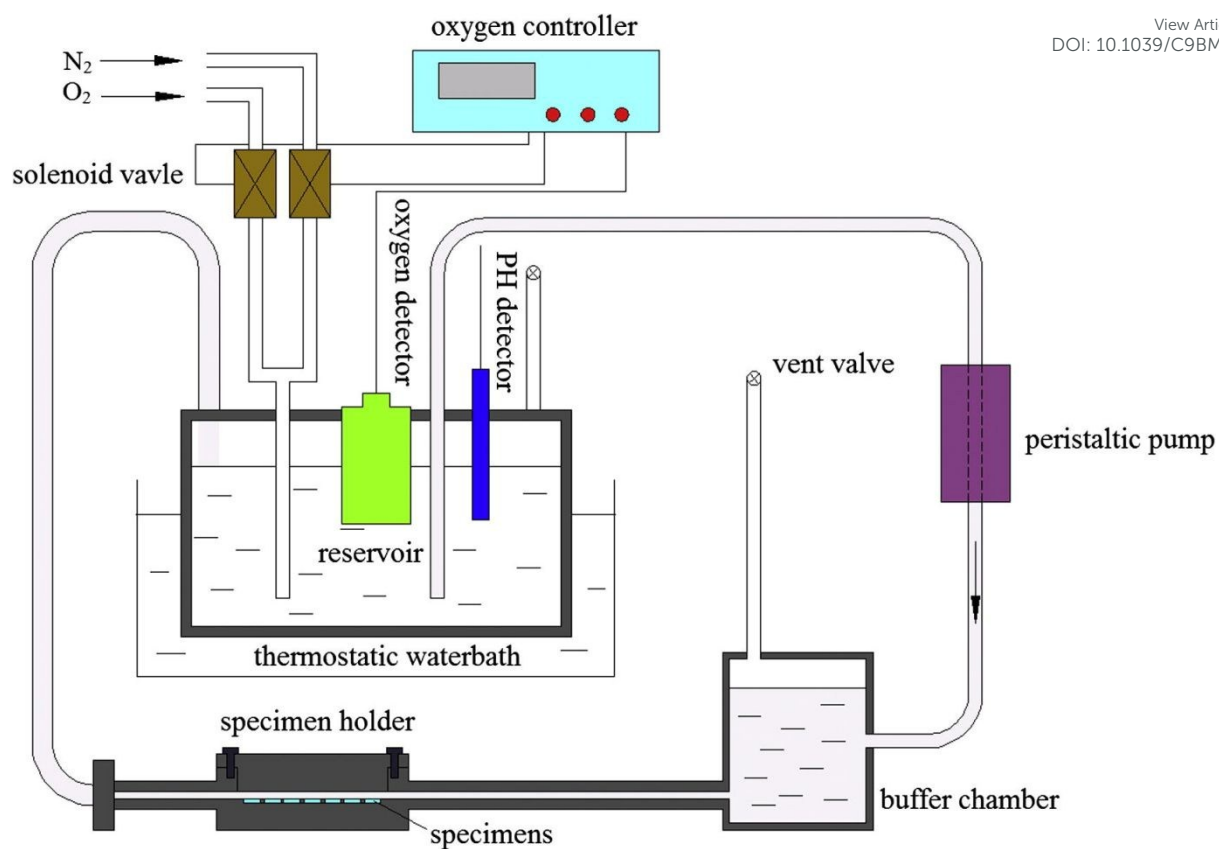


Figure 1.



View Article Online
DOI: 10.1039/C9BM00289H

Figure 2.

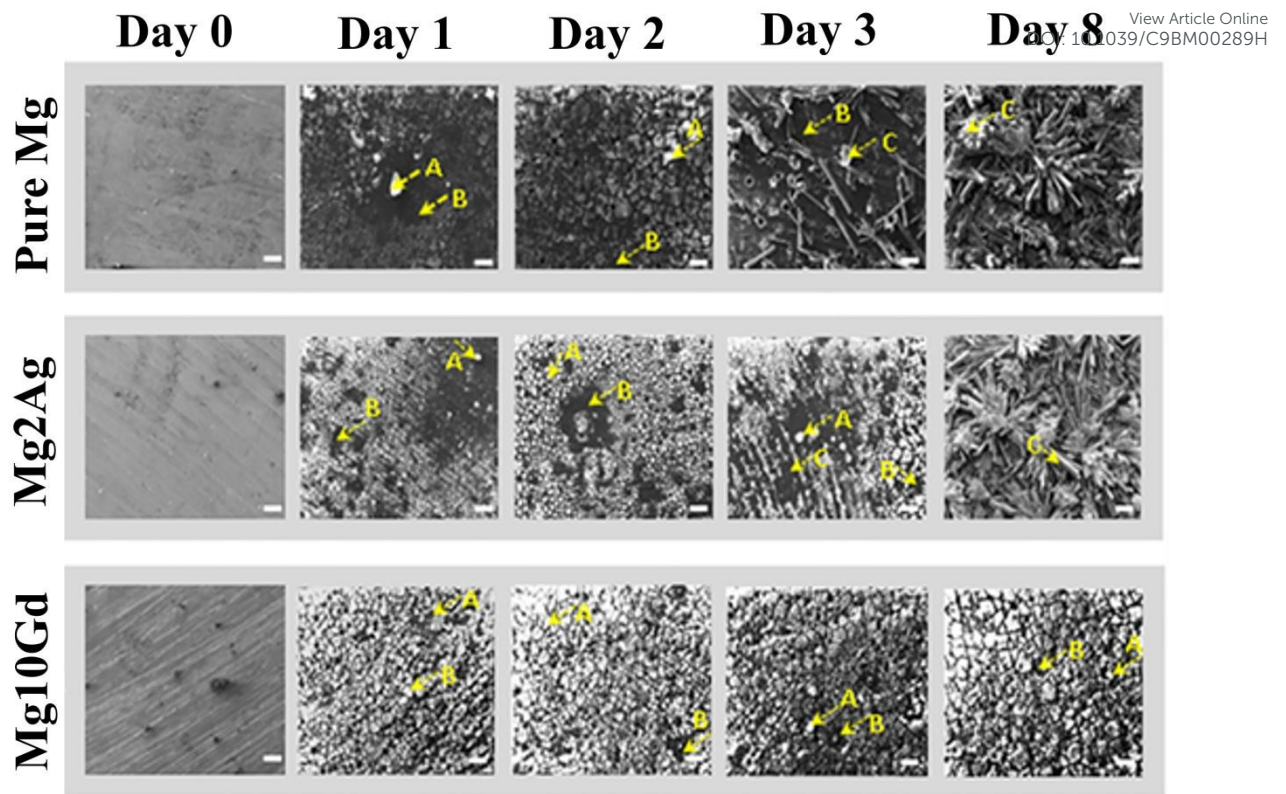


Figure 3.

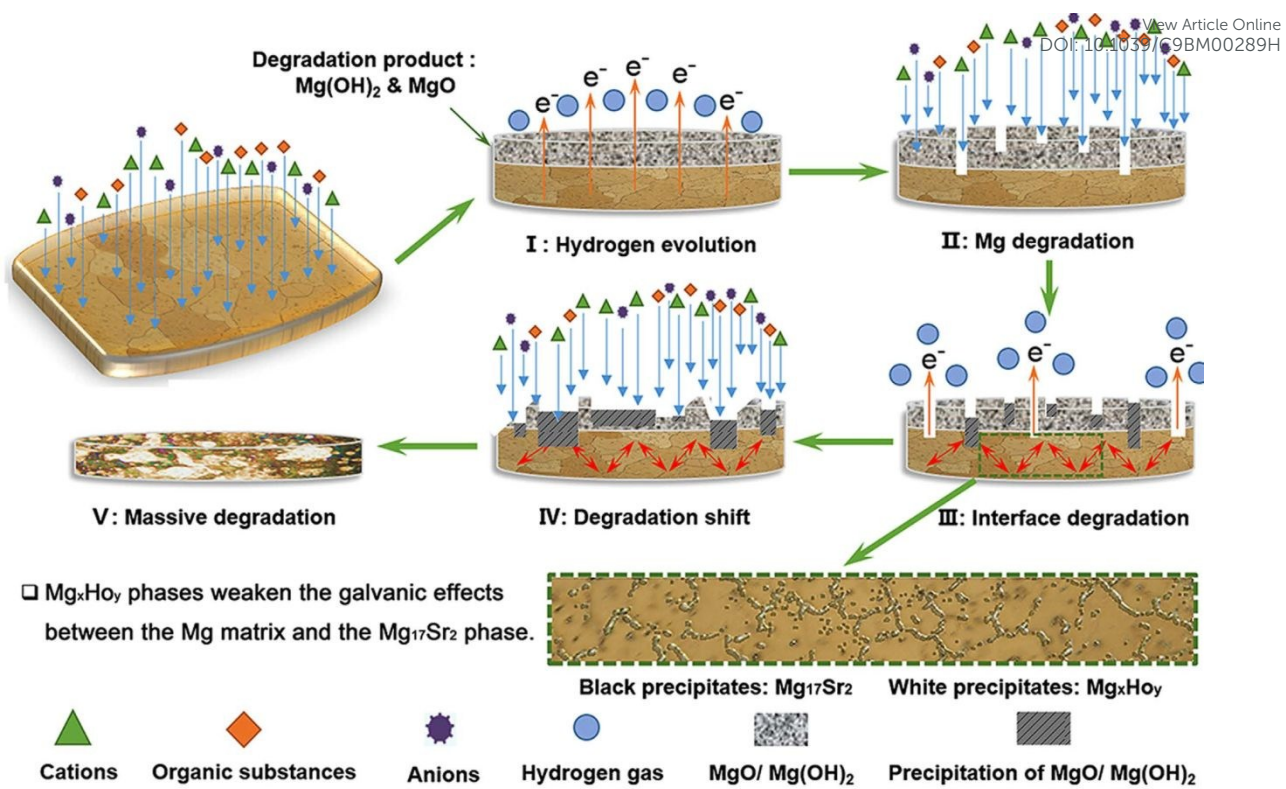


Figure 4.

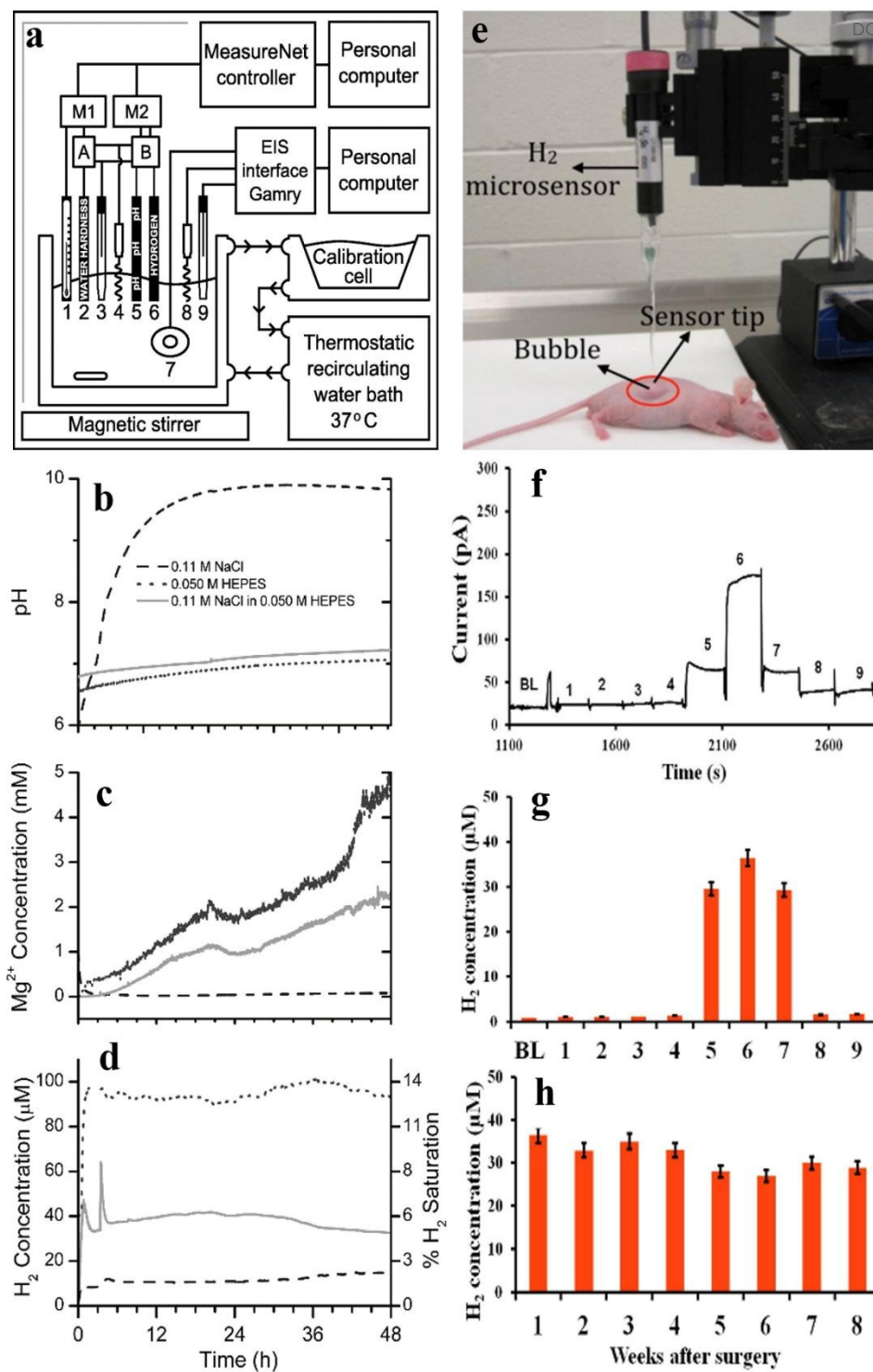


Figure 5.

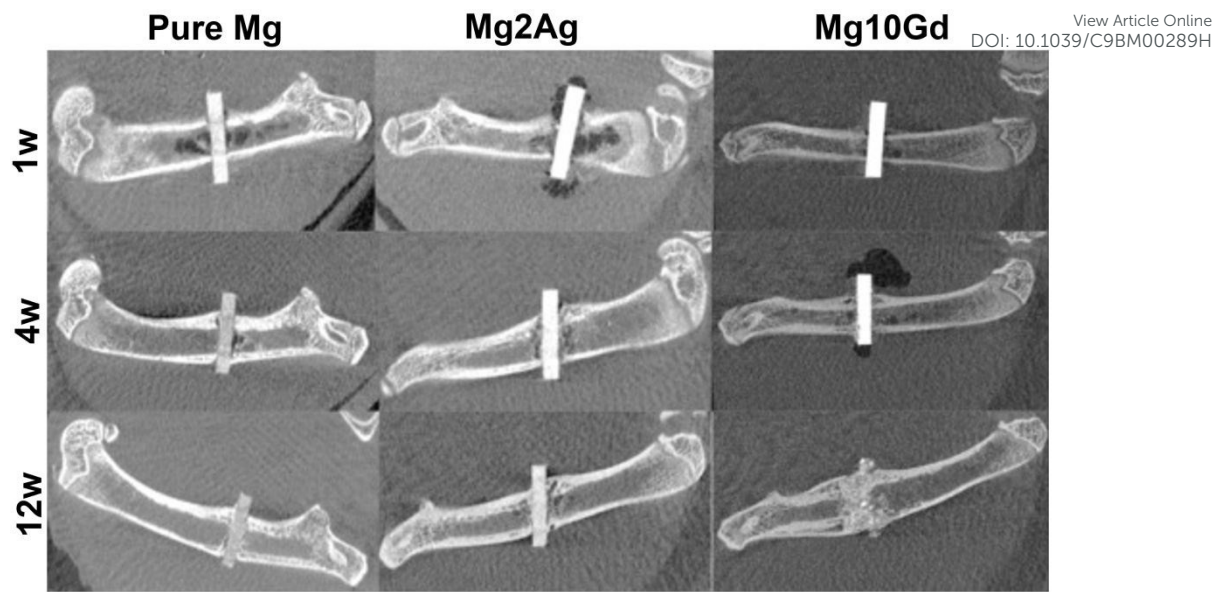


Figure 6.

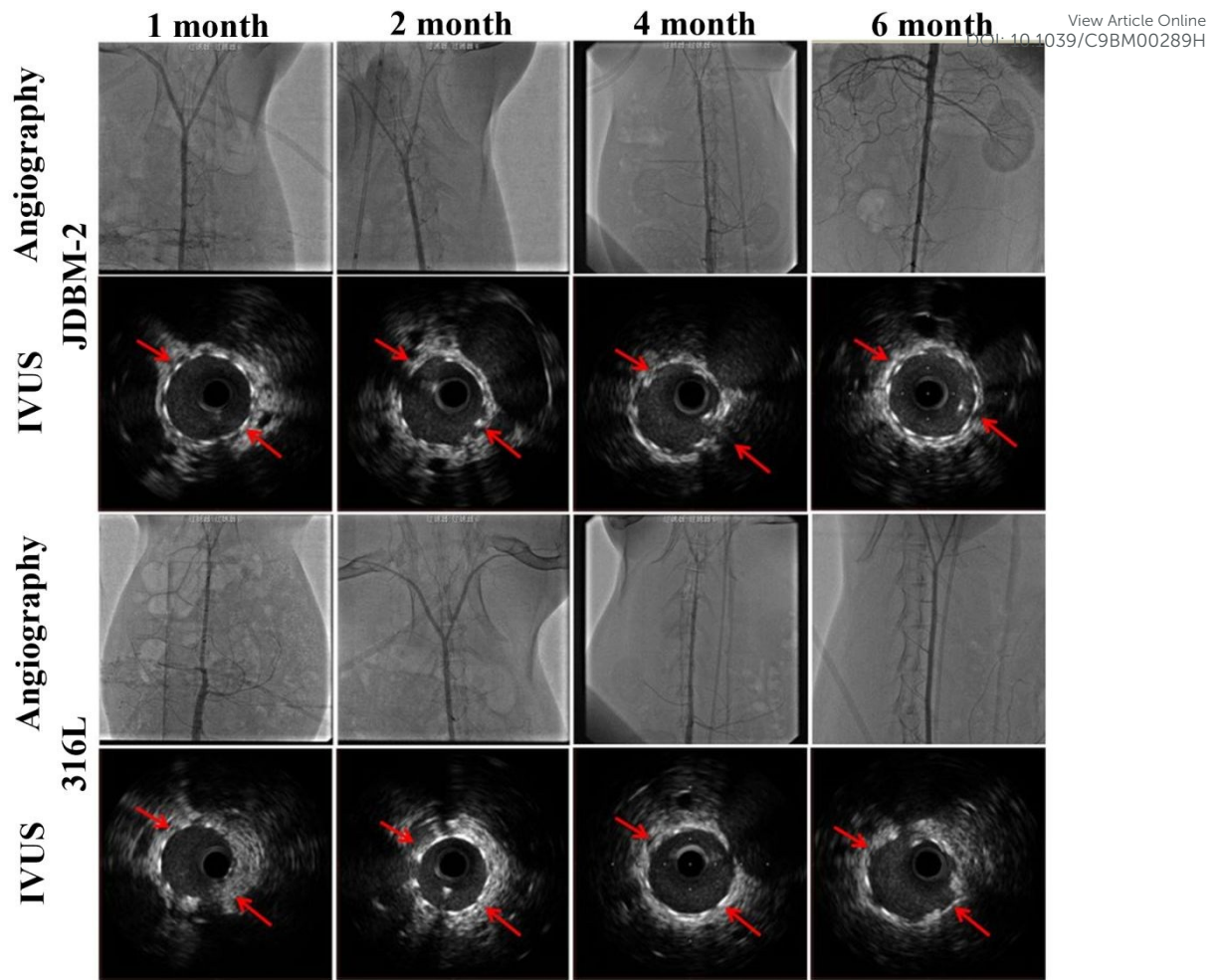


Figure 7.

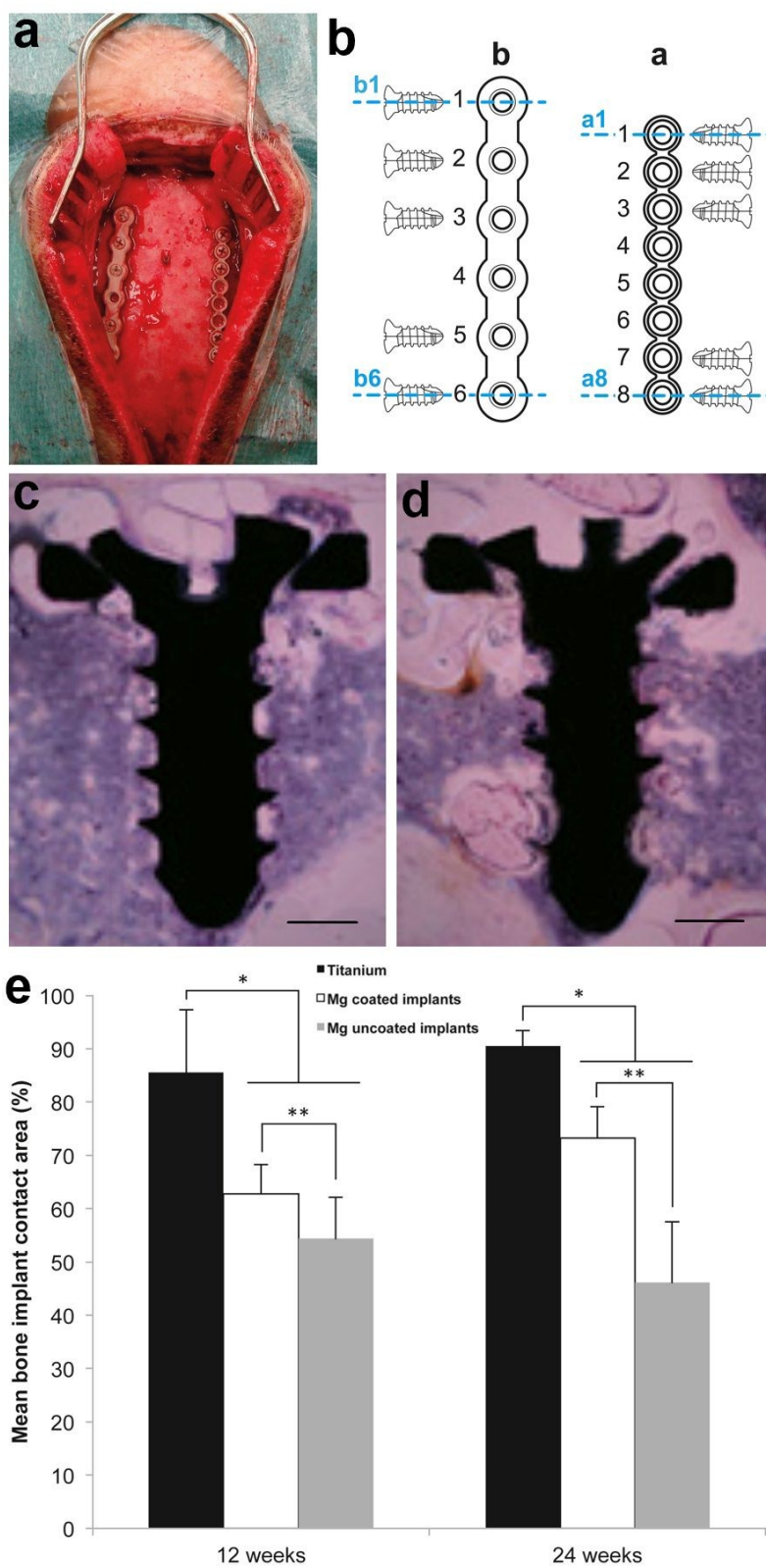


Figure 8.

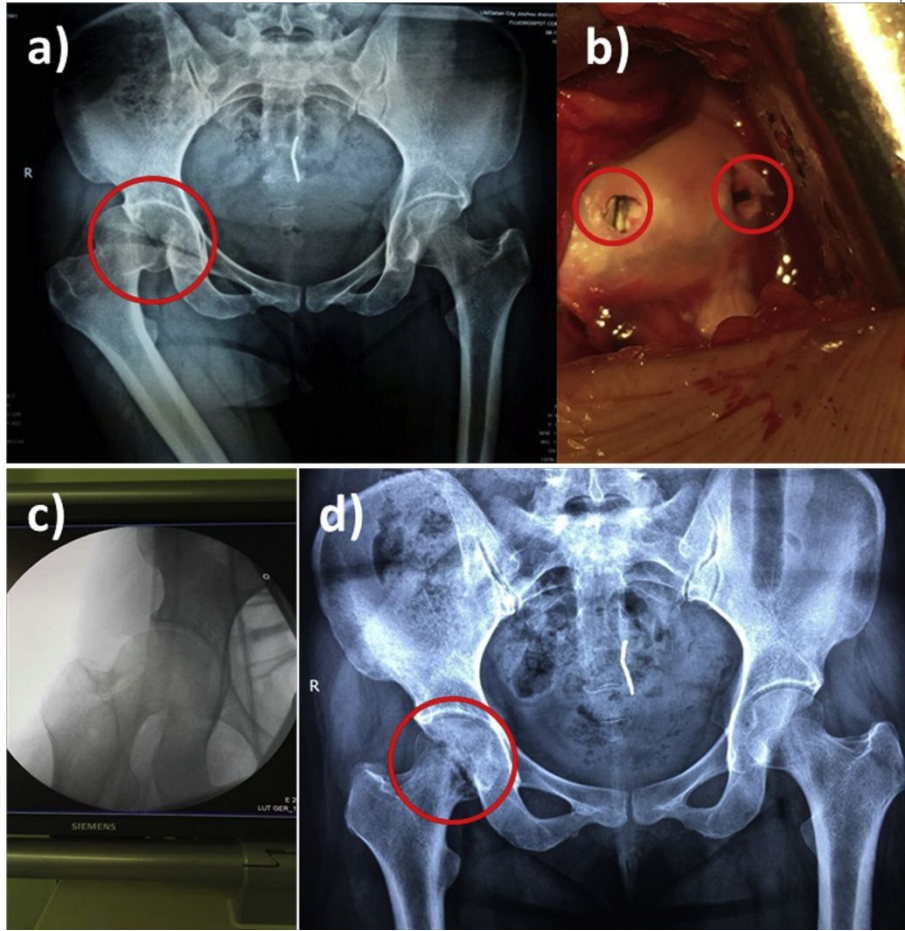


Figure 9.

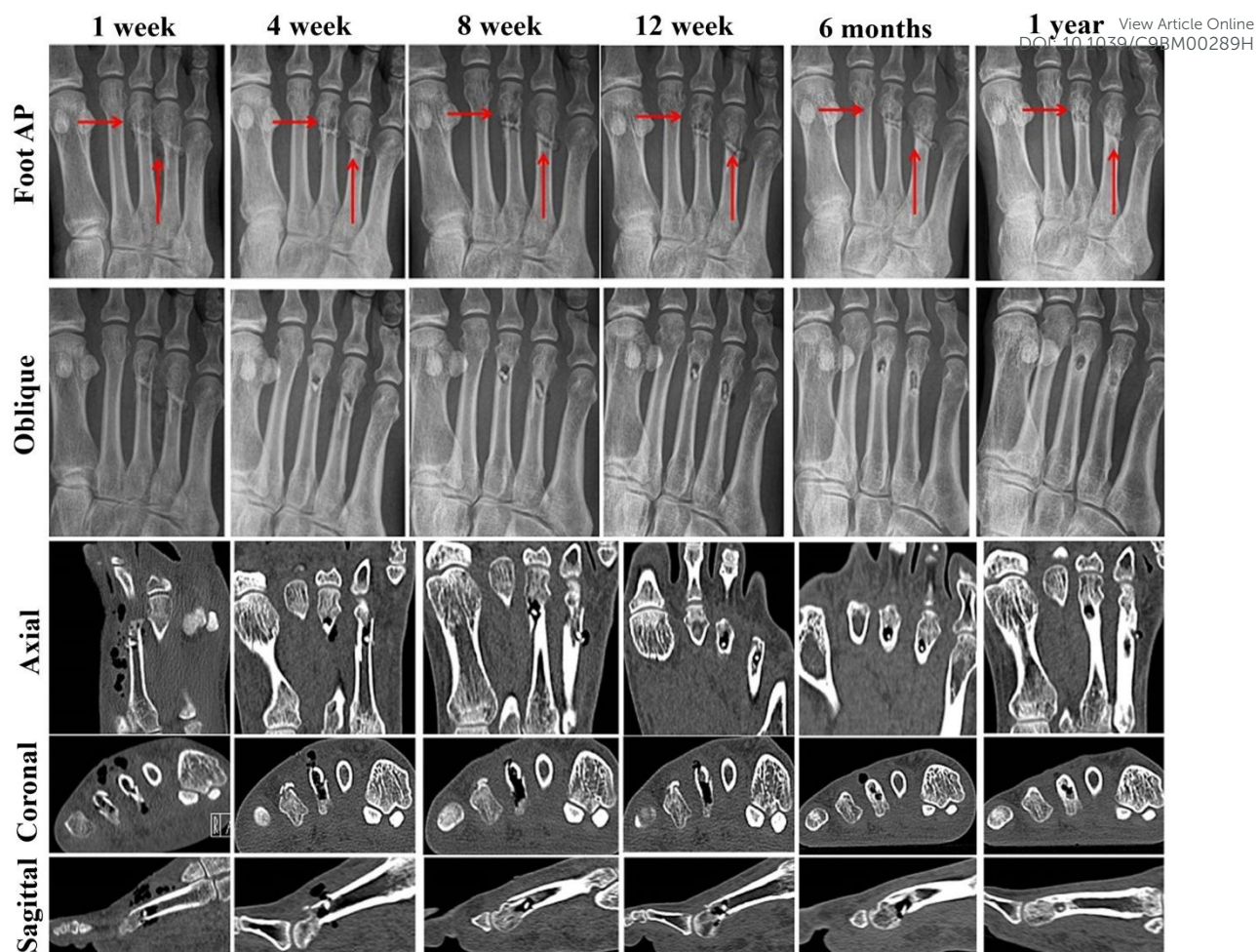
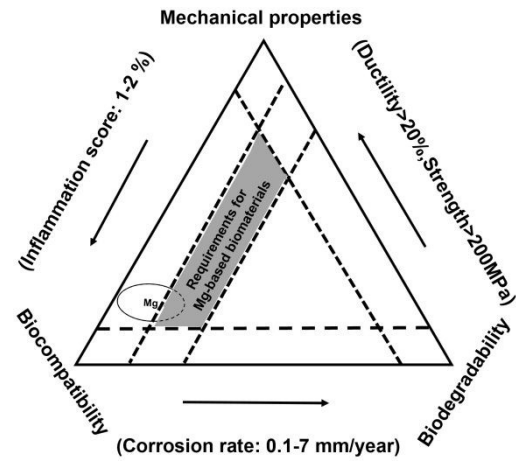


Figure 10.

Table of contents entry



This review presents the operation procedures of commonly used standard methods for assessment of Mg-based biomaterials from bench to clinic.